Atmospheric
Chemistry
and Physics

Application of WRF/Chem-MADRID and WRF/Polyphemus in Europe – Part 2: Evaluation of chemical concentrations and sensitivity simulations

Y. Zhang[1], K. Sartelet[2], S. Zhu[1], W. Wang[1,4], S.-Y. Wu[3], X. Zhang[1], K. Wang[1], P. Tran[2], C. Seigneur[2], and Z.-F. Wang[4]

[1]Department of Marine, Earth, and Atmospheric Sciences, North Carolina State University, Raleigh, NC 27695, USA
[2]CEREA (Atmospheric Environment Center), Joint Laboratory of École des Ponts ParisTech and EDF R&D, Université Paris-Est, 77455 Marne-la-Vallée, France
[3]Department of Air Quality and Environmental Management, Clark County, NV, USA
[4]Institute of Atmospheric Physics, Chinese Academy of Science, Beijing, China

Correspondence to: Y. Zhang (yzhang9@ncsu.edu)

Abstract. An offline-coupled model (WRF/Polyphemus) and an online-coupled model (WRF/Chem-MADRID) are applied to simulate air quality in July 2001 at horizontal grid resolutions of 0.5° and 0.125° over Western Europe. The model performance is evaluated against available surface and satellite observations. The two models simulate different concentrations in terms of domainwide performance statistics, spatial distribution, temporal variations, and column abundance. WRF/Chem-MADRID at 0.5° gives higher values than WRF/Polyphemus for the domainwide mean and over polluted regions in Central and southern Europe for all surface concentrations and column variables except for the tropospheric ozone residual (TOR). Compared with observations, WRF/Polyphemus gives better statistical performance for daily HNO_3, SO_2, and NO_2 at the European Monitoring and Evaluation Programme (EMEP) sites, maximum 1 h O_3 at the AirBase sites, $PM_{2.5}$ at the AirBase sites, maximum 8 h O_3 and PM_{10} composition at all sites, column abundance of CO, NO_2, TOR, and aerosol optical depth (AOD), whereas WRF/Chem-MADRID gives better statistical performance for NH_3, hourly SO_2, NO_2, and O_3 at the AirBase and BDQA (Base de données de la qualité de l'air) sites, maximum 1 h O_3 at the BDQA and EMEP sites, and PM_{10} at all sites. WRF/Chem-MADRID generally reproduces well the observed high hourly concentrations of SO_2 and NO_2 at most sites except for extremely high episodes at a few sites,

and WRF/Polyphemus performs well for hourly SO_2 concentrations at most rural or background sites where pollutant levels are relatively low, but it underpredicts the observed hourly NO_2 concentrations at most sites. Both models generally capture well the daytime maximum 8 h O_3 concentrations and diurnal variations of O_3 with more accurate peak daytime and minimal nighttime values by WRF/Chem-MADRID, but neither model reproduces extremely low nighttime O_3 concentrations at several urban and suburban sites due to underpredictions of NO_x and thus insufficient titration of O_3 at night. WRF/Polyphemus gives more accurate concentrations of $PM_{2.5}$, and WRF/Chem-MADRID reproduces better the observations of PM_{10} concentrations at all sites. The differences between model predictions and observations are mostly caused by inaccurate representations of emissions of gaseous precursors and primary PM species, as well as biases in the meteorological predictions. The differences in model predictions are caused by differences in the heights of the first model layers and thickness of each layer that affect vertical distributions of emissions, model treatments such as dry/wet deposition, heterogeneous chemistry, and aerosol and cloud, as well as model inputs such as emissions of soil dust and sea salt and chemical boundary conditions of CO and O_3 used in both models.

WRF/Chem-MADRID shows a higher sensitivity to grid resolution than WRF/Polyphemus at all sites. For both

models, the use of a finer grid resolution generally leads to an overall better statistical performance for most variables, with greater spatial details and an overall better agreement in temporal variations and magnitudes at most sites. The use of online biogenic volatile organic compound (BVOC) emissions gives better statistical performance for hourly and maximum 8 h O_3 and $PM_{2.5}$ and generally better agreement with their observed temporal variations at most sites. Because it is an online model, WRF/Chem-MADRID offers the advantage of accounting for various feedbacks between meteorology and chemical species. However, this model comparison suggests that atmospheric pollutant concentrations are most sensitive in state-of-the-science air quality models to vertical structure, inputs, and parameterizations for dry/wet removal of gases and particles in the model.

1 Introduction

Uncertainties in air quality modeling are high and exist in both offline- and online-coupled air quality models (AQMs). The uncertainties lie in model inputs such as meteorological fields, land use, emissions, and chemical initial and boundary conditions (ICs and BCs), model treatments such as inaccurate or missing atmospheric processes, as well as model simulation setup such as horizontal and vertical grid resolutions. In the framework of the Air Quality Model Evaluation International Initiative (AQMEII) project, Sartelet et al. (2012) found that for O_3, $PM_{2.5}$, and PM_{10} over Europe differences between the WRF/Polyphemus simulations using different anthropogenic or biogenic emission schemes are much smaller than the differences among the different AQMEII models. A number of studies examined which physical parameterizations, numerical approximations and boundary conditions affect pollutant concentrations the most over Europe (e.g., Pérez et al., 2006; Roustan et al., 2010). For example, Roustan et al. (2010) found that for most pollutants the modeling of the vertical diffusivity and the vertical resolution affects the simulated concentrations the most. However, the relative impact of the different parameterizations varies with the pollutants considered. Using the same model configuration, Real et al. (2011) found that the impact of aerosols on photolysis rates and, therefore, on gas-phase chemistry and aerosol concentrations is also important. Differences in ozone (O_3) and PM concentrations were found to occur depending on the gas-phase chemical scheme (Kim et al., 2009, 2011). A number of studies examined the sensitivity of offline-coupled AQM predictions to horizontal grid resolutions. For example, Queen and Zhang (2008) found that the simulation at a fine grid resolution of 4 km better captured the mesoscale convection and thus predicted more accurate precipitation and wet deposition of chemical species in summer than the simulations at 12 or 36 km grid resolutions. Several studies, on the other hand, showed that

a coarser grid resolution provided similar or even better air quality predictions than a finer grid resolution (Mathur et al., 2005; Arunachalam et al., 2006; Cohan et al., 2006; Zhang et al., 2006; Queen and Zhang, 2008; Liu et al., 2010). Bailey et al. (2007) and Valari and Menut (2008) found that model results do not improve monotonously with resolution. In all of these studies, meteorology is computed off-line, i.e., independently of the chemical transport model (CTM) calculation. It is assumed that there is no feedback between aerosol and meteorology.

Compared with offline-coupled models, the major advantage of the online-coupled meteorology and chemistry models is their capabilities to simulate not only pollutant concentrations but also aerosol direct and indirect feedbacks. For example, using WRF/Chem, Zhang et al. (2010) found that aerosols reduce incoming solar radiation by -16%, 2 m temperatures by up to $0.37\,^\circ\text{C}$, and daily precipitation by up to $19.4\,\text{mm day}^{-1}$ and lead to 500–$5000\,\text{cm}^{-3}$ cloud condensation nuclei (CCN) at a supersaturation of 1% over most land areas in July over the continental US. Such feedbacks can change the abundance and lifetimes of chemical species such as CO, NO_2, NH_3, and O_3 through changing radiation, atmospheric stability, and the rates of many meteorologically dependent chemical and microphysical processes (Zhang et al., 2012a, b). Forkel et al. (2012) estimated the direct and indirect effects of aerosols on surface O_3 and PM_{10} concentrations for June and July 2006 over Europe and found that the agreement between observed and simulated global radiation over Europe was better for cloudy conditions, and the monthly PM_{10} concentration increased by 1–$3\,\mu\text{g m}^{-3}$ when the indirect effect was taken into account. Tuccella et al. (2012) reported significant underpredictions of sulfate by WRF/Chem without aerosol feedbacks and attributed this result to the missing aqueous-phase oxidation of SO_2 by H_2O_2 and O_3, a process that is not included in the standard configuration of WRF/Chem without aerosol–cloud feedbacks.

Similar to offline-coupled AQMs, online-coupled AQMs are subject to all aforementioned uncertainties and additional uncertainties in the meteorology–chemistry feedback mechanisms such as aerosol direct effects on radiation, photolysis rates, and planetary boundary layer (PBL) meteorology and indirect effects on cloud formation and precipitation through acting as cloud condensation nuclei (CCN) and ice nuclei (IN). Furthermore, the uncertainties in those feedback mechanisms may be amplified by uncertainties in model inputs such as biogenic emissions and other model treatments such as gas-phase mechanisms, aerosol treatments, and cloud chemistry and microphysics, with latter uncertainties propagating into the former uncertainties through a sequence of chain effects. For example, Zhang et al. (2012a) applied an online-coupled WRF/Chem-MADRID model over the continental US and reported large differences in shortwave radiation and near-surface temperature and relative humidity at individual sites under cloudy conditions among the three simulations with three different gas-phase mechanisms. They
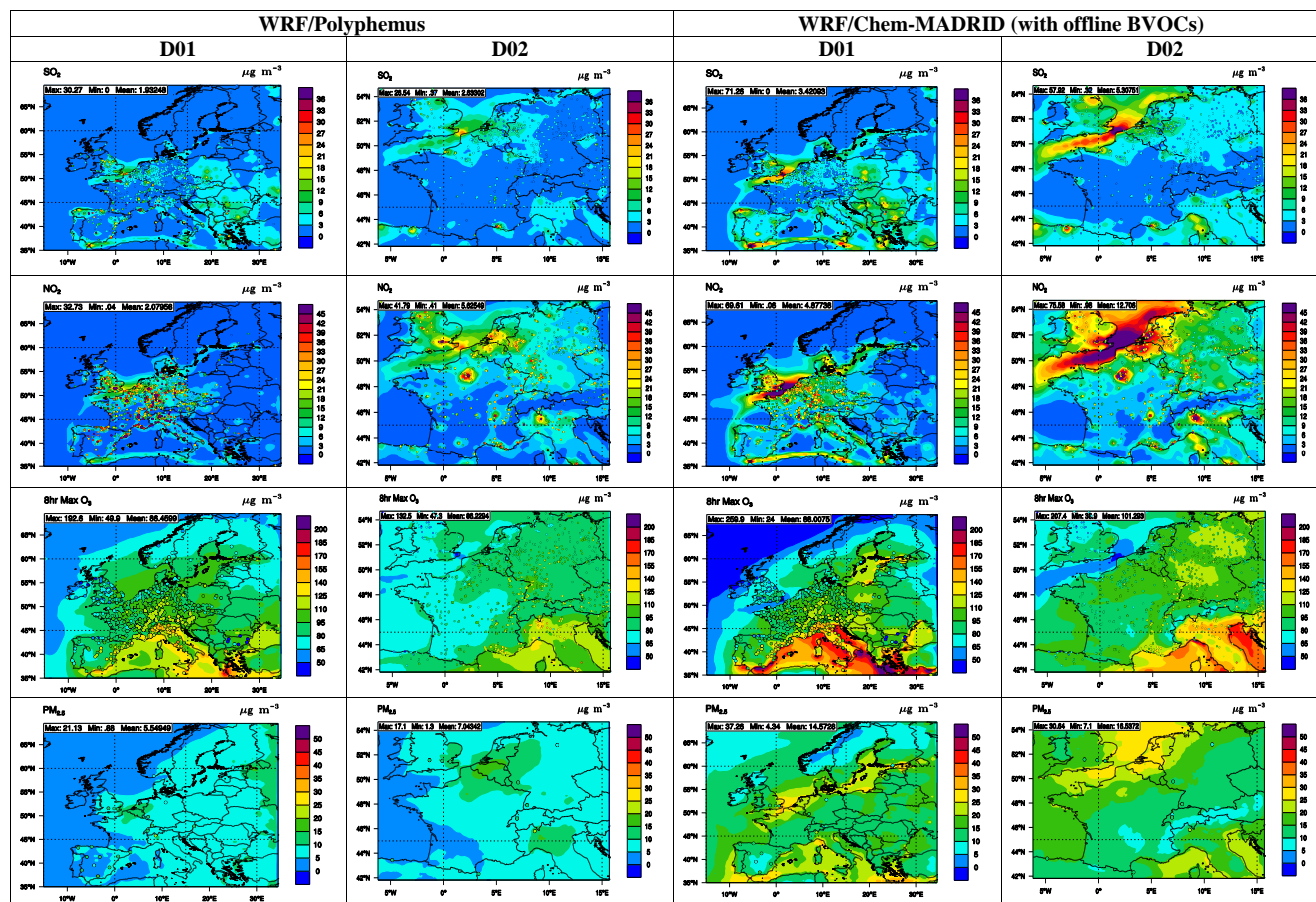
Fig. 1. Simulated concentrations of SO_2, NO_2, maximum 8 h O_3, and $PM_{2.5}$ by WRF/Chem-MADRID and WRF/Polyphemus overlaid with observations in July 2001 over D01 and D02.

found that different gas-phase mechanisms lead to different aerosol mass and number concentrations, which in turn lead to different predictions of CCN and cloud droplet number concentration (CDNC) and cloud formation, and subsequently differences in shortwave radiation and PBL meteorology that are affected by cloud formation. These differences are caused by the sensitivity of the chain effects of feedback mechanisms among H_2SO_4 vapor, $PM_{2.5}$ number, CCN, and CDNC through gas-phase chemistry and new particle formation via homogeneous nucleation, aerosol growth, and aerosol activation by cloud droplets. The sensitivity of online-coupled air quality models to horizontal grid resolutions has also been studied (e.g., Misenis and Zhang, 2010; Wolke et al., 2012). For example, Wolke et al. (2012) found that the use of finer grid resolutions in their online-coupled model (i.e., COSMO-MUSCAT) can directly affect the meteorological predictions, and the calculated emission and deposition rates.

In this work, the simulations using the offline-coupled model (i.e., WRF/Polyphemus) and the online-coupled model (WRF/Chem-MADRID) are performed for July 2001

over double-nested domains: D01 and D02 as shown in Fig. 1 of Part 1 (Zhang et al., 2013), at horizontal grid resolutions of 0.5° and 0.125°, respectively. Part 2 describes the evaluation and comparison of the chemical concentrations simulated by the two models, the sensitivity of chemical concentrations to horizontal grid resolutions for both models and to biogenic emissions for WRF/Chem-MADRID, as well as the effect of aerosol and meteorology interactions on air pollutant concentrations simulated using WRF/Chem-MADRID. The objectives are to evaluate the current offline- and online-coupled model capabilities of reproducing observations, to understand the most influential factors that cause differences in model predictions from both models, and to identify potential areas of model improvements.

Table 1. Comparison of performance statistics of WRF/Polyphemus and WRF/Chem-MADRID over D01[1].

Variable	Network	Data pair	Mean Obs[2]	Mean Mod[2,3]				Corr[3]				NMB[3] (%)				NME[3] (%)			
				WP	WC-S	WC-G	WC-M	WP	WC-S	WC-G	WC-M	WP	WC-S	WC-G	WC-M	WP	WC-S	WC-G	WC-M
Hourly NH_3	AIRBASE	5355	9.3	5.8	5.9	5.8	5.8	0.2	0.3	0.3	0.3	−38.0	−36.5	−37.2	−37.4	80.5	84.2	84.5	84.5
Daily NH_3	EMEP	251	2.5	2.1	2.4	2.4	2.3	0.9	0.8	0.8	0.8	−15.8	−5.2	−6.5	−7.2	50.6	71.1	70.0	69.8
Daily HNO_3	EMEP	250	0.5	1.3	1.5	2.0	2.3	0.4	0.4	0.4	0.4	135.9	175.9	277.2	323.4	161.1	207.0	300.3	344.0
Hourly SO_2	AIRBASE	577595	5.1	3.5	5.9	5.8	5.8	0.2	0.2	0.2	0.2	−30.4	16.5	14.7	15.1	72.9	93.1	92.2	92.5
	BDQA	32073	5.3	3.4	5.6	5.5	5.5	0.2	0.2	0.2	0.2	−36.1	6.4	4.9	5.4	81.2	98.9	98.4	98.5
Daily SO_2	EMEP	1432	1.0	2.3	3.7	3.6	3.6	0.5	0.5	0.5	0.5	120.2	256.9	249.3	245.2	138.4	265.7	258.4	254.5
Hourly NO_2	AIRBASE	741439	17.4	7.6	14.6	14.5	14.5	0.3	0.3	0.3	0.3	−56.2	−15.7	−16.4	−16.8	70.3	72.5	71.9	72.2
	BDQA	55326	15.9	7.2	13.5	13.2	13.1	0.2	0.2	0.2	0.2	−54.7	−15.4	−17.0	−17.6	75.3	81.9	82.2	82.2
Daily NO_2	EMEP	1091	4.7	4.1	8.4	8.4	8.6	0.6	0.4	0.4	0.4	−12.0	78.3	77.3	81.7	50.8	111.5	111.1	113.6
Hourly O_3	AIRBASE	779596	67.9	80.9	78.7	70.8	77.3	0.5	0.7	0.7	0.7	19.1	15.9	4.2	13.8	40.3	36.1	32.7	34.6
	BDQA	97266	71.0	79.0	78.2	69.4	76.0	0.6	0.7	0.7	0.7	11.2	10.1	−2.3	7.0	34.4	31.4	29.5	29.9
	EMEP	82306	74.2	78.8	77.5	71.5	69.8	0.6	0.6	0.6	0.6	6.1	4.3	−3.7	−6.0	28.0	29.0	27.5	27.7
Max 1-h O_3	AIRBASE	33271	105.4	103.9	112.4	99.9	109.3	0.6	0.7	0.7	0.7	−1.3	6.4	−5.4	3.5	20.4	20.7	19.3	19.0
	BDQA	4135	110.8	102.5	113.8	99.7	109.2	0.7	0.8	0.8	0.8	−7.5	2.6	−10.2	−1.6	19.7	18.6	18.7	17.0
	EMEP	3499	101.1	96.8	103.9	94.4	92.2	0.6	0.7	0.7	0.7	−4.2	2.7	−6.7	−8.9	18.5	19.7	18.3	18.8
Max 8-h O_3	AIRBASE	32730	94.8	99.9	104.8	93.2	102.1	0.6	0.7	0.7	0.7	5.6	10.5	−1.7	7.7	21.6	22.2	19.5	20.3
	BDQA	4080	99.8	98.2	105.9	92.8	101.8	0.7	0.8	0.8	0.8	−1.6	6.1	−7.0	2.0	18.8	19.1	18.0	17.1
	EMEP	3433	92.7	93.3	97.1	88.5	86.5	0.6	0.7	0.7	0.7	0.6	4.9	−4.4	−6.6	18.8	20.0	18.1	18.4
Hourly $PM_{2.5}$	AIRBASE	2618	12.1	11.3	25.3	21.1	21.4	0.5	0.4	0.4	0.5	−7.0	109.4	74.7	77.4	42.6	125.6	94.3	94.8
Daily $PM_{2.5}$	AIRBASE	110	12.0	11.2	25.6	21.3	21.6	0.7	0.7	0.7	0.7	−7.4	112.7	77.0	79.6	29.7	115.5	81.5	82.7
	EMEP	537	12.0	8.4	14.8	14.9	14.9	0.6	0.5	0.5	0.5	−30.4	23.3	23.8	24.4	41.5	48.5	48.9	48.6
Hourly PM_{10}	AIRBASE	214203	24.3	11.9	21.5	21.2	21.7	0.3	0.3	0.3	0.3	−51.1	−11.8	−12.9	−10.7	59.1	54.1	53.2	54.1
	BDQA	22667	19.4	12.3	23.5	23.4	24.1	0.4	0.3	0.3	0.3	−36.5	20.8	20.4	24.1	52.8	64.2	63.3	65.5
Daily PM_{10}	AIRBASE	9215	24.4	11.9	21.5	21.2	21.8	0.4	0.4	0.4	0.4	−51.2	−11.8	−12.8	−10.7	53.6	36.1	35.5	35.4
	BDQA	997	19.0	12.2	23.2	23.1	23.8	0.5	0.5	0.5	0.5	−36.2	24.9	24.6	28.3	42.9	46.7	45.7	47.6
	EMEP	811	17.4	10.5	18.8	18.9	18.9	0.6	0.4	0.4	0.4	−39.5	8.3	8.6	8.7	46.4	45.7	45.4	44.9
Daily PM_{10} SO_4^{2-}	AIRBASE	606	2.1	2.1	3.1	3.3	3.3	0.6	0.7	0.7	0.7	0.2	49.1	58.5	58.1	54.7	74.1	78.7	78.6
	EMEP	1570	2.7	2.2	3.7	4.1	4.2	0.6	0.6	0.6	0.6	−16.0	39.0	52.1	58.4	44.5	59.6	67.9	72.9
Daily PM_{10} NO_3^-	AIRBASE	271	2.7	3.7	8.5	8.4	8.7	0.8	0.7	0.7	0.7	37.2	214.4	211.4	221.7	58.2	220.7	217.5	227.0
	EMEP	553	1.4	1.0	2.7	2.9	3.1	0.6	0.5	0.5	0.5	−23.7	95.1	116.2	127.8	74.9	148.5	158.4	164.8
Daily PM_{10} NH_4^+	AIRBASE	271	1.7	2.0	2.9	3.0	3.0	0.7	0.8	0.8	0.8	12.9	69.6	71.1	75.3	35.4	79.6	80.1	83.8
	EMEP	449	1.1	1.0	1.3	1.5	1.5	0.7	0.7	0.7	0.7	−4.4	21.9	36.1	42.7	46.9	65.9	69.9	73.6
Daily PM_{10} Na^+	EMEP	164	0.3	0.5	1.7	1.7	1.7	0.7	0.7	0.7	0.7	71.1	474.2	477.5	477.9	112.7	474.2	477.5	477.9
Daily PM_{10} Cl^-	AIRBASE	163	0.7	2.2	3.7	3.7	3.7	0.7	0.7	0.7	0.7	235.7	452.0	456.8	453.0	251.5	461.3	466.1	462.4
	EMEP	102	0.2	0.7	1.0	1.0	1.0	0.4	0.6	0.6	0.6	274.3	449.5	454.1	443.3	321.3	460.9	465.3	455.0
Column CO[4]	MOPPIT	4963	1.44	1.5	2.2	2.1	2.1	0.1	0.3	0.1	0.2	5.3	50.9	43.0	45.3	25.8	51.0	43.6	45.7
Column NO_2[4]	GOME	5234	1.9	1.6	2.7	2.8	2.8	0.8	0.8	0.8	0.8	−13.7	45.1	52.0	49.2	41.7	59.1	64.2	61.4
TOR	TOMS	2160	43.7	55.5	30.3	30.1	30.5	0.6	0.7	0.7	0.7	26.8	−30.6	−31.2	−30.2	26.8	30.6	31.2	30.2
AOD	MODIS	5398	0.19	0.42	0.43	0.41	0.41	0.60	0.28	0.31	0.33	125.0	129.6	115.2	116.2	125.3	131.3	117.6	118.5

[1] WP – WRF/Polyphemus; the WRF/Chem-MADRID simulations with three BVOC emissions include: WC-S – offline BVOC emissions of Simpson et al. (1999); WC-G – online Guenther et al. (1995); WC-M – online Guenther et al. (2006) (i.e., MEGAN);

[2] unit of concentration is $\mu g\,m^{-3}$;

[3] the best statistics among 4 runs is in green, corr – correlation coefficient, NMB – normalized mean bias, and NME – normalized mean error;

[4] the column CO and NO_2 abundance and tropospheric ozone residual (TOR) values are in 1×10^{18} molec cm^{-2}, 1×10^{15} molec cm^{-2}, and Dobson unit (DU), respectively.

2 Evaluation and intercomparison of WRF/Chem and WRF/Polyphemus

2.1 Spatial distribution and domainwide performance statistics

Figures 1 and 2 show simulated spatial distributions of concentrations of SO_2, NO_2, maximum 8 h O_3, and 24 h average $PM_{2.5}$, PM_{10}, and major PM_{10} composition (SO_4^{2-}, NO_3^-, NH_4^+, and total organic matter (TOM)) by WRF/Polyphemus and WRF/Chem-MADRID overlaid with observations over D01 and D02 at horizontal grid resolutions of 0.5° and 0.125° in July 2001. The corresponding domainwide performance statistics for those species and additional species such as NH_3, HNO_3, and other PM_{10} components (Na^+ and Cl^-) is shown in Table 1. The results over D01 are discussed below, and those over D02 are discussed in Sect. 3.1. The observed concentrations of SO_2, NO_2, O_3, and $PM_{2.5}$ are higher in several areas in Central and southern Europe than in northern Europe (i.e., the Nordic countries such as Denmark, Norway, Sweden, and Finland and Baltic countries such as Esto-

nia, Latvia, and Lithuania) because of higher pollutant precursor concentrations and weather conditions that are more conducive to O_3 and secondary $PM_{2.5}$ production at these mid-latitudes. The spatial distributions of SO_2 concentrations predicted by both models are overall similar and consistent with the spatial distribution of SO_2 emissions inland and over shipping routes. WRF/Chem-MADRID predicts higher SO_2 concentrations and greater gradients in several areas, including the English Channel, the shipping routes in the Mediterranean Sea off the south of Spain, Italy, and Greece, the northwestern corner of Spain, and the southern portions of Poland, Romania, and Bulgaria. Spatially, WRF/Chem-MADRID also predicts higher NO_2 concentrations in larger areas, particularly over areas with high NO_2 emissions, including the English Channel and southern UK, northern France, northern Italy, Germany, Belgium, the Netherlands, Denmark, the Baltic Sea areas off the coast of Sweden, as well as the shipping routes in the Mediterranean Sea. Differences in SO_2 and NO_2 concentrations predicted by both models are likely caused by several factors, including differences in heights in the first model layer and the thickness
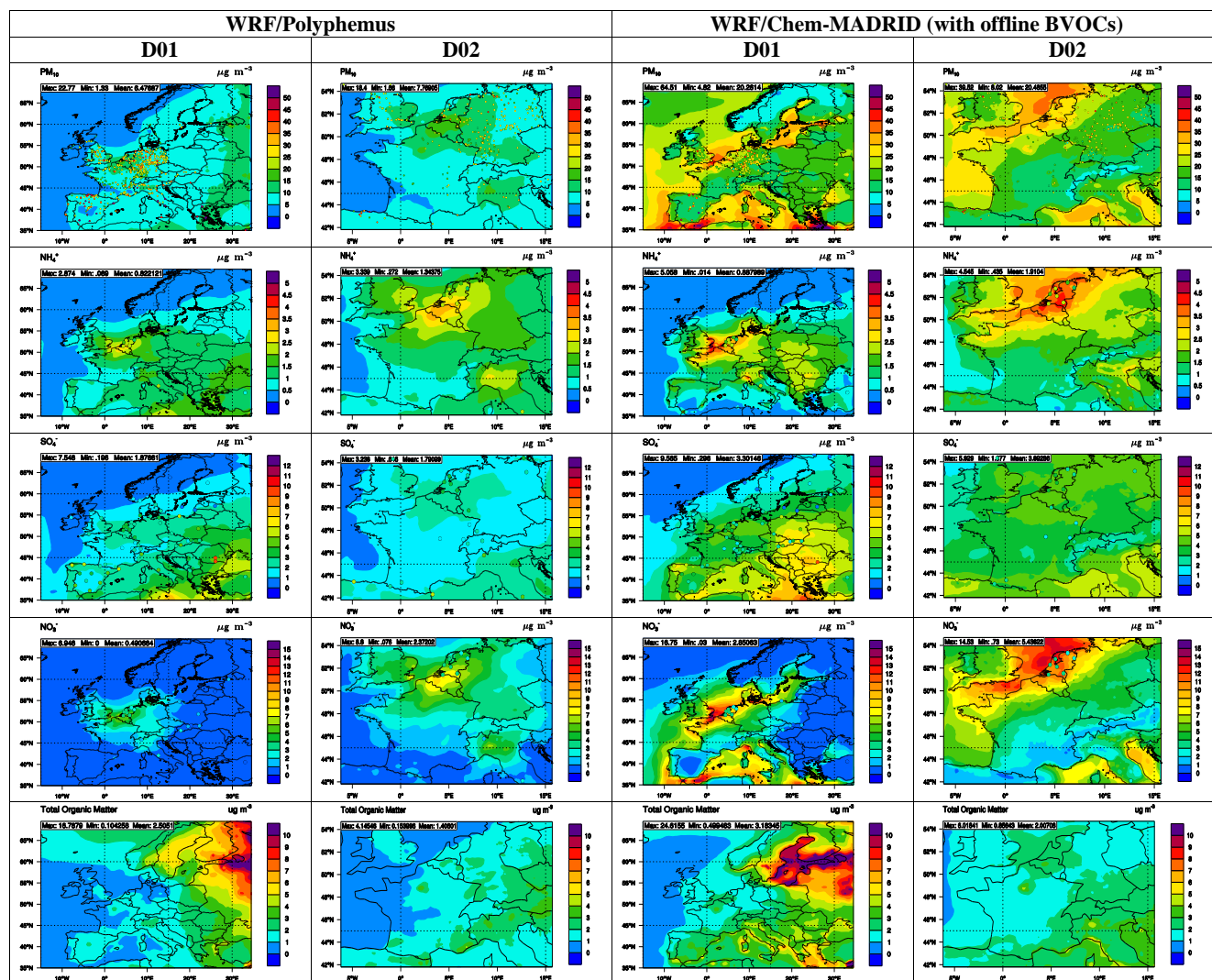
Fig. 2. Simulated concentrations of PM_{10} and its components, NH_{4+}, SO_4^{2-}, NO_{3-}, and organic matter (OM) by WRF/Polyphemus and WRF/Chem-MADRID overlaid with observations in July 2001 over D01 and D02. No observations were available for OM.

of each layer, that affect the vertical distributions of emissions, dry and wet deposition treatments, and aerosol treatments as described in Part 1 (Zhang et al., 2013). Given the same surface emissions, lower heights in the first model layer in WRF/Chem can lead to higher surface concentrations. Different thickness of each layer in both models can also lead to differences in concentrations in the surface and upper layers. Compared with WRF/Polyphemus, WRF/Chem-MADRID gives much lower dry deposition fluxes for gases (see Part 1, Zhang et al., 2013), leading to higher concentrations of SO_2, NO_x, and other gaseous species such as NH_3, HNO_3, O_3, and OH radicals. Consequently, the levels of those gaseous precursors for aerosol thermodynamic partitioning and the levels of aqueous-phase oxidants such as O_3 and H_2O_2 for aqueous-phase formation of secondary aerosols are also higher in WRF/Chem-MADRID, leading

to higher production of SO_4^{2-}, NO_3^-, and NH_4^+. Further, homogeneous binary nucleation of sulfuric acid (H_2SO_4) and water vapor (H_2O) and aerosol thermodynamics of Na^+ and Cl^- are treated in WRF/Chem-MADRID, but not treated in WRF/Polyphemus. As a result of nucleation treatments, WRF/Chem-MADRID gives higher PM number concentrations and cloud droplet number concentrations, which can enhance cloud formation and thus aqueous-phase formation of SO_4^{2-}. Inclusion of Na^+ and Cl^- in aerosol thermodynamics calculations in WRF/Chem-MADRID may enhance the formation of NO_3^-. The heterogeneous reactions of NO_3 and N_2O_5 treated in WRF/Polyphemus provide additional pathways to remove reactive nitrogen, therefore decreasing NO_2 and increasing NO_3^- in the particulate phase, as shown by Roustan et al. (2010). Such different treatments help explain in part lower concentrations of NO_2 predicted by

WRF/Polyphemus than by WRF/Chem-MADRID. For domainwide performance statistics, WRF/Polyphemus underpredicts observed SO_2 concentrations at the AirBase and BDQA (Base de données de la qualité de l'air) sites with normalized mean biases (NMBs) of -30.4% and -36.1%, respectively, and overpredicts those at the European Monitoring and Evaluation Programme (EMEP) sites with an NMB of 120.2%, whereas WRF/Chem-MADRID overpredicts observations at all sites, particularly at the EMEP sites with an NMB of 256.9%. WRF/Polyphemus also underpredicts observed NO_2 concentrations, particularly at the AirBase and BDQA sites, with NMBs of -56.2% and -54.7%, respectively. WRF/Chem-MADRID performs much better over the AirBase and BDQA sites with NMBs of -15.7% and -15.4%, respectively. However, it significantly overpredicts those at the EMEP sites with an NMB of 78.3%. Uncertainties in the EMEP emissions of SO_2 and NO_x in terms of total amount and spatial and vertical distributions as reported in several studies (e.g., de Meij et al., 2006; Mallet and Sportisse, 2006) may contribute to the discrepancies between observations and predictions by both models. For example, 50% of SO_2 and NO_2 emissions in the EMEP inventories are assumed to be emitted at $\sim150\,m$ (de Meij et al., 2006), which may explain in part the underpredictions in surface concentrations of NO_2 by both models and in those of SO_2 by Polyphemus. The EMEP sites are mostly rural background sites, and the AirBase and BDQA sites also include suburban and urban background sites. WRF/Polyphemus tends to perform better for SO_2 and NO_2 at rural sites, while WRF/Chem-MADRID tends to perform better at suburban and urban background sites.

For maximum 1 h O_3, WRF/Chem-MADRID performs better than WRF/Polyphemus, with small overpredictions against AirBase and small to moderate underpredictions against BDQA and EMEP. For maximum 8 h O_3, WRF/Polyphemus slightly underpredicts with NMBs of -1.6% to 5.6%, and WRF/Chem-MADRID slightly overpredicts with NMBs of $4.9–10.5\%$ at all sites. The differences between the predicted O_3 concentrations by the two models may be mainly explained by the differences in dry deposition treatments used in both models (as described in Part 1). Compared with WRF/Chem-MADRID, WRF/Polyphemus gives higher dry deposition fluxes for O_3, leading to lower O_3 concentrations. Spatially, both models predict much larger concentrations of maximum 8 h O_3 (see Fig. 1) and maximum 1 h O_3 (figure not shown but very similar to those for maximum 8 h O_3) in the Mediterranean Sea, Italy, Greece, and Turkey ($>110\,\mu g\,m^{-3}$), with larger magnitudes, and in several additional areas such as the Baltic Sea, central Poland, and western Hungary by WRF/Chem-MADRID due to lower dry deposition fluxes of O_3 and its precursor gases. These high O_3 concentrations are caused by high pollutant precursors and the summer weather conditions that favor the formation of O_3. Despite overpredictions, both models predict enhanced near-surface O_3 concen-

trations in southern Sweden and Finland, and Baltic Europe, consistent with observed historic O_3 trends reported by Engardt et al. (2009). The elevated O_3 levels reflect the advection of O_3-laden air from continental Europe after periods of O_3 buildup.

For $PM_{2.5}$ concentrations, WRF/Polyphemus moderately underpredicts them with NMBs of -30.4% and -7.4% at the EMEP and AirBase sites (in particular over Spain), respectively, for daily concentrations and -7.0% at the EMEP sites for hourly concentrations. WRF/Chem-MADRID significantly overpredicts hourly and daily $PM_{2.5}$ concentrations at the AirBase sites with NMBs of 109.4% and 112.7% and moderately overpredicts daily $PM_{2.5}$ concentrations with an NMB of 23.3% . Spatially, WRF/Chem-MADRID generates much higher $PM_{2.5}$ concentrations over the whole domain than WRF/Polyphemus, with domain-average values of 14.6 and $5.5\,\mu g\,m^{-3}$, respectively. The highest $PM_{2.5}$ concentrations are predicted along the shipping routes in the Mediterranean Sea, the English Channel, and the Baltic Sea. Similarly to O_3 predictions, both models predict enhanced levels of $PM_{2.5}$ in the Nordic and Baltic countries, reflecting the impact of long-range transport of $PM_{2.5}$ and its precursors from Central Europe to this region. For PM_{10} concentrations, WRF/Polyphemus significantly underpredicts them at all sites (in particular over Spain) with NMBs of -51.2 to -36.2%. WRF/Chem-MADRID performs better with NMBs of -11.8% to 24.9% for daily concentrations and -11.8% to 20.8% for hourly concentrations, mainly because of the overprediction of $PM_{2.5}$ and sea-salt concentrations as well as the inclusion of mineral dust emissions. The spatial distributions of PM_{10} concentrations are overall similar to those of $PM_{2.5}$ concentrations in both models. Similar to $PM_{2.5}$ concentrations, WRF/Chem-MADRID predicts three times higher PM_{10} concentrations over the whole domain than WRF/Polyphemus, with domain-average values of 20.3 and $6.5\,\mu g\,m^{-3}$, respectively, and the highest concentrations along the shipping routes. The domainwide mean concentrations of coarse PM (i.e., $PM_{10-2.5}$) are $1\,\mu g\,m^{-3}$ for WRF/Polyphemus and $5.7\,\mu g\,m^{-3}$ for WRF/Chem-MADRID over D01. WRF/Chem-MADRID predicts higher $PM_{10-2.5}$ concentrations than WRF/Polyphemus due to the online generation of mineral dust emissions from land types that can possibly emit dust particles such as shrubland, barren, or sparsely vegetated land and sea-salt emissions that are higher than offline sea-salt emissions used in WRF/Polyphemus. Differences in natural emissions of sea salt and mineral dust may also contribute to differences in predicted $PM_{2.5}$ concentrations, as a small portion of those emissions are in the size range of $PM_{2.5}$. Although dust particle emissions from the Sahara desert are not explicitly simulated because the simulation domain does not cover Sahara desert, WRF/Chem-MADRID uses chemical BCs from the global-through-urban WRF/Chem (GU-WRF/Chem) of Zhang et al. (2012b), which simulates mineral dust emissions from all dust source regions including the Sahara desert,

and it also simulates soil dust emissions from the aforementioned land types within the simulation domain. The enhanced PM_{10} concentrations simulated by WRF/Chem-MADRID are consistent with several studies that accounted for contributions of mineral dust to PM_{10} (e.g., Jiménez-Guerrero et al., 2008). In WRF/Polyphemus, $PM_{10-2.5}$ results primarily from the offline sea-salt emissions. Although the Goddard Chemistry Aerosol Radiation and Transport (GOCART, Chin et al., 2000) also accounted for the contributions of Saharan dust, those values represented high dust events and were unrealistically high. They were divided by 4 to represent the boundary conditions of coarse PM in WRF/Polyphemus following Sartelet et al. (2007), resulting in small differences between simulated PM_{10} and $PM_{2.5}$ concentrations over southern Europe.

In addition to higher dust and sea-salt concentrations, higher concentrations of secondary inorganic aerosols such as NH_4^+, SO_4^{2-}, and NO_3^-, secondary organic aerosols (SOAs), and primary PM (e.g., elemental carbon (EC), primary organic carbon (POC), dust, and sea salt) contribute to higher $PM_{2.5}$ and PM_{10} concentrations by WRF/Chem-MADRID. Those higher concentrations result from the differences in heights of the first model layers and thickness of each layer, which affects the vertical distributions of emissions of primary PM and gaseous precursors of secondary PM as mentioned previously and in model treatments including dry and wet depositions of $PM_{2.5}$ and PM_{10} compositions, inorganic aerosol thermodynamics, heterogeneous chemistry, SOA, and aerosol–cloud interactions. For example, compared with WRF/Polyphemus, WRF/Chem-MADRID may estimate lower dry deposition velocities and lower wet scavenging coefficients for PM species, leading to higher PM concentrations. WRF/Chem-MADRID overpredicts the concentrations of secondary inorganic aerosol species, whereas to a lesser extent WRF/Polyphemus either underpredicts (e.g., SO_4^{2-} and NO_3^- at the EMEP sites) or overpredicts (e.g., Na^+ and Cl^- at all sites and NH_4^+ and NO_3^- at the AirBase sites). For example, the NMBs of SO_4^{2-} concentrations are -16.0% to 0.2% for WRF/Polyphemus and 39.0% to 49.1% for WRF/Chem-MADRID. At the EMEP sites, small to moderate underpredictions occur in the NH_3 concentrations with an NMB of -15.8% for WRF/Polyphemus and -5.2% for WRF/Chem-MADRID. The HNO_3 concentrations are significantly overpredicted (with NMBs of 135.9% for WRF/Polyphemus and 175.9% for WRF/Chem-MADRID). Those model biases contribute to biases in the simulated concentrations of NH_4^+ and NO_3^-, with a small to moderate underprediction (with NMBs of -4.4% and -23.7%, respectively) by WRF/Polyphemus and the moderate to large overpredictions (with NMBs of 21.9% and 95.1%, respectively) by WRF/Chem-MADRID. At the AirBase sites, larger underpredictions occur in the NH_3 concentrations with NMBs of -38.0% for WRF/Polyphemus and -36.5% for

WRF/Chem-MADRID. Although there are no observational data for HNO_3 from AirBase, moderate to large overpredictions of NH_4^+ and NO_3^- concentrations (NMBs of 12.9% and 37.2% for WRF/Polyphemus and 69.6% and 214.4% for WRF/Chem-MADRID, respectively) imply an overprediction of HNO_3 concentrations. They also indicate a NH_4^+-rich environment in which ammonium nitrate (NH_4NO_3) formation is limited by the formation of HNO_3 in the simulation domain, which is consistent with the findings of Sartelet et al. (2007). Both models predict high concentrations of SOA (thus TOM) over regions with high isoprene and terpene emissions, such as the northeastern portion of the domain, which dominates the concentrations of TOM. WRF/Chem-MADRID also predicts high concentrations of SOA in the southern portion of the domain where biogenic volatile organic compound (VOC) emissions are also high. WRF/Chem-MADRID gives a higher domain-averaged TOM concentration than WRF/Polyphemus due to higher gaseous oxidant levels and differences in the SOA treatments in both models. Note that no observations for SOA and TOM are available for evaluation.

3 Evaluation of temporal variations at specific sites

3.1 Description of selected sites

A total of 16 and 21 sites have been selected from 3 observational databases (AirBase, EMEP, and BDQA) for detailed temporal analyses of chemical predictions of gaseous (e.g., SO_2, NO_2, and O_3) and PM (e.g., $PM_{2.5}$ and PM_{10}) pollutants, respectively. These sites and their characteristics are summarized in Table 3. Among the 16 sites selected for analyses of SO_2, NO_2, and O_3, 8 sites (Melun, Nord-Est Alsace, and Sommet Puy-de-Dôme, France; Deuselbach, Germany; Ispra, Italy; Celje, Slovenia; Harwell, UK; and Avenida Gasteiz, Spain) are in D02, and 8 sites (Rörvik, Femman, and Södermalm, Sweden; Birkenes, Norway; Topolniky, Slovakia; Beato, Custóias, and Ermesinde, Portugal) are in D01 but outside D02. Among the 21 sites selected for analysis of $PM_{2.5}$ and PM_{10}, 13 sites (Tremblay-en-France and Ternay, France; Deuselbach and Langenbrugge, Germany; Payerne and Chaumont, Switzerland; Ispra, Italy; Celje, Slovenia; Harwell, Rochester Stoke, and London Bloomsbury, UK; and Cabo de Creus and Niembro, Spain) are in D02, and 8 sites (Celje, Slovenia; Sundsvall and Södermalm, Sweden; Birkenes, Norway; Mansikkala and Kallio_2, Finland; Illmitz, Austria; Ermesinde, Portugal) are in D01 but outside D02. Because of a lack of concurrent measurements of gaseous and PM concentrations at the same or colocated sites, the sites selected for gaseous and PM measurements are mostly different. Among the 32 sites selected, only 7 sites are common to both gaseous and PM measurements including Deuselbach, Ispra, Celje, Harwell, Södermalm, Birkenes, and Ermesinde. Only 6 sites are co-
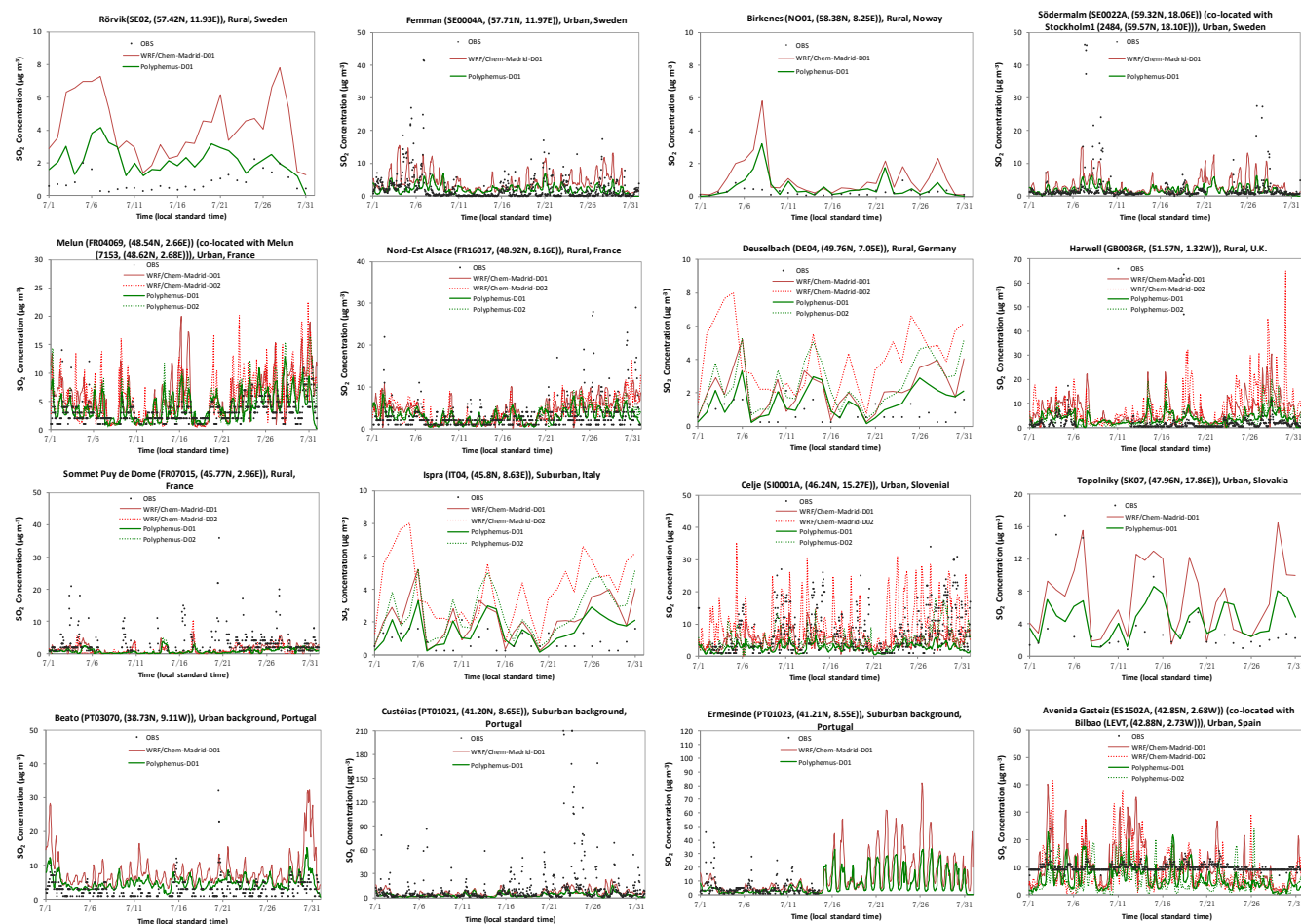
Fig. 3. Simulated and observed hourly or daily concentrations of SO$_2$ in July 2001 at selected sites over D01 and D02 in four latitude bands: 57–60° N, 48–52° N, 45–48° N, and 38–43° N (rows 1, 2, 3, and 4, respectively).

located with the selected meteorological sites from the NCEP or the ECA&D databases (see Table 5 in Part 1) including 2 AirBase/BDQA sites (Melun and Tremblay-en-France) in France and 4 AirBase sites (Düsseldorf-Lörick in Germany, Avenida Gasteiz in Spain, Södermalm in Sweden, and London Bloomsbury in the UK). Melun (FR04069) is co-located with the NCEP site (Melun, 7153) and the ECA&D site (Brétigny-sur-Orge, 000764). Tremblay-en-France (FR04319) is co-located with the NCEP site (Charles de Gaulle, 7157). Düsseldorf-Lörick is co-located with the NCEP site (Düsseldorf 1 (10400)/Düsseldorf 210400 (EDDL)). Avenida Gasteiz (ES1502A) is co-located with the NCEP site Bilbao (LEVT). Södermalm (SE0022A) is co-located with the NCEP site Stockholm 1 (02484) and the ECA&D site Stockholm (000010). London Bloomsbury (GB0566A) in the UK is co-located with the NCEP sites London 1 (3779) and London 2 (3781).

These sites are selected from 14 countries for their geographical and topographical representations. They are classified into 6 urban sites (Melun, Topolniky, Celje, Avenida Gasteiz, Femman, Södermalm), 4 suburban sites (Ternay, Tremblay-en-France, Ispra, Payerne), 13 rural sites (Keldsnor, Nord-Est Alsace, Sommet Puy-de-Dôme, Deuselbach, Langenbrugge, Birkenes, Cabo de Creus, Els Torms, Niembro, Rörvik, Chaumont, Harwell, and Rochester Stoke), and 9 background sites (Illmitz, Mansikkala, Kallio_2, Sundsvall, London Bloomsbury, Düsseldorf-Lörick, Beato, Custóias, and Ermesinde). Among those background sites, 1 is a rural background site (Illmitz), 4 are urban background sites (Kallio_2, London Bloomsbury, Beato, and Sundsvall), and the remaining 4 are suburban background sites. Among all sites, there are 8 sites located 200 m above sea level (ASL), including Sommet Puy-de-Dôme (1460 m), Chaumont (1130 m), Avenida Gasteiz (517 m), Payerne (510 m), Deuselbach (480 m), Celje (240 m), Ternay (235 m), and Ispra (209 m). The altitude, location, and topography affect the climatic conditions at all selected sites. Climatic conditions at these selected sites include Western European oceanic climate (i.e., Melun, Nord-Est Alsace, Sommet Puy-de-Dôme, Ternay, and Tremblay-en-France,

France; Harwell, Rochester Stoke, and London Bloomsbury, UK; Avenida Gasteiz and Niembro, Spain; Illmitz, Austria; Deuselbach and Langenbrugge, Germany; Ispra, Italy; Birkenes, Norway; Rörvik and Femman, Sweden; and Payerne, Switzerland), continental or subtropical Mediterranean climate (Cabo de Creus, Spain; Beato, Custóias, and Ermesinde, Portugal), humid continental climate (Kallio, Finland; Södermalm, Sweden; and Chaumont, Switzerland), warm temperate climate (e.g., Keldsnor, Denmark; Topolniky, Slovakia; Celje, Slovenia), and subarctic climate (Mansikkala, Finland), borderline between oceanic and humid subtropical climate (Ternay, France), and borderline between subarctic and cold continental climate (Sundsvall, Sweden). Similar to the site selection for meteorological evaluation in Part 1, in addition to the representativeness of those sites in terms of climatic, geographical, and topographical characteristics, chemical data availability and completeness are also part of the consideration for site selections.

3.1.1 Simulations over D01 at a horizontal grid resolution of 0.5°

Figure 3 shows simulated and observed hourly concentrations of SO_2 at 16 selected sites in four latitude bands: 57–60° N, 48–52° N, 45–48° N, and 38–43° N. The model performance varies with locations substantially. In the northern latitude band (57–60° N), both models overpredict the concentrations of SO_2 on a typical day but fail to reproduce the observed extremely high concentrations of SO_2 during several pollution episodes at 2 urban sites in Sweden: Femman on 4–6, 20, and 27 July and Södermalm on 7–9 and 26–28 July, with much better agreement on high SO_2 concentrations by WRF/Chem-MADRID than WRF/Polyphemus. Femman is a roof site in Gothenburg, the second largest city in southwestern Sweden. The Gothenburg area is known to have relatively limited dispersion due to complex terrain (i.e., valleys carved down into a flat plateau and its proximity to the sea). This topography favors the development of stable air and inversions inside the valleys (Haeger-Eugensson et al., 2010). The special topography and the stable, low wind meteorological conditions, coupled with high emissions of SO_2, lead to extremely high SO_2 episodes on some days in the Gothenburg area. Södermalm is located in central Stockholm on the south-central east coast of Sweden. Stockholm is the capital and the largest city of Sweden and constitutes the most populated urban area in Scandinavia. The topography of Stockholm is relatively smooth, without dominating ridges or valleys. However, Stockholm has a hemiboreal humid continental climate featuring a warm to hot summer. The wind speeds in Stockholm are typically low (mostly <4 m s^{-1}) (see Fig. 13 in Part 1). The hot, humid, and low wind summer coupled with high emissions favors the accumulation of air pollutants such as SO_2 in Stockholm. As shown in Figures 9, 13, and 15 in Part 1, WRF captures well the meteorological conditions in Stockholm.

The failure of reproducing the extremely high SO_2 by both models at Södermalm and Femman is primarily caused by the missing of the episodic emissions during a few days. WRF/Chem-MADRID gives much higher SO_2 concentrations than WRF/Polyphemus for the reasons mentioned previously. At the 2 rural sites Rörvik, Sweden and Birkenes, Norway, both models significantly overpredict, with better agreement by WRF/Polyphemus. In the central latitude band (48–52° N), both models overpredict at the urban site Melun and the rural site Nord-Est Alsace in France with better agreement by WRF/Polyphemus with observed low and average concentrations on most days and by WRF/Chem-MADRID with observed high concentrations (e.g., during 2–5 July at Melun and during 2, 6, 21, 25–26, and 30–31 July at Nord-Est Alsace). As shown in Fig. 12 in Part 1, wind speeds are significantly underpredicted at Melun, which may explain in part the overpredictions in the SO_2 concentrations at Melun due to underestimated dispersion. At the other 2 rural sites (Deuselbach, Germany, and Harwell, UK), both models significantly overpredict SO_2 concentrations, with fewer overpredictions by WRF/Polyphemus. In the central south latitude band (45–48° N), while large overpredictions by both models occur at an urban site (Topolniky, Slovakia) and a suburban site (Ispra, Italy), underpredictions occur at a rural mountain site (Sommet Puy-de-Dôme) on the top of the Puy-de-Dôme, a large lava dome and extinct volcano in south-central France where observed SO_2 concentrations are typically high (>5 µg m^{-3}) and can reach 36 µg m^{-3} due to regional emissions from industrial sources. At the urban site Celje in Slovenia where observed SO_2 concentrations are high (mostly in the range of 5–34 µg m^{-3}), while WRF/Polyphemus underpredicts, WRF/Chem-MADRID reproduces well the observed high SO_2 concentrations. Celje has a climate that is in a transition between continental and alpine influenced by urban heat island. It is located in a basin with regular temperature inversions and prevailing weak local winds (Otorepec and Gale, 2004), which favors pollutant buildup. The main sources of air pollution include traffic (in particular, diesel vehicles), poor oil burning in some residential areas, burning of high sulfur content coal in small domestic furnaces, and industrial sources (e.g., titanium production plant (1 % of the world production), H_2SO_4 production, iron works, enamel factory and ceramic industry) (Otorepec and Gale, 2004). In the southern latitude band (38–43° N), both models overpredict at the urban site Avenida Gasteiz in Spain, and at the urban background site Beato in Portugal, where the observed SO_2 concentrations are typically low to moderate (mostly <4 and 11 µg m^{-3}, respectively). As shown in Figs. 9, 13, and 15 in the Part 1 paper, WRF simulates 10 m wind speeds well but largely underpredicts peak 2 m temperatures and overpredicts precipitation on 6–9 and 15–21 July at Avenida Gasteiz. In addition to inaccurate emissions of SO_2, the underpredictions in peak 2 m temperatures may partly explain the peak SO_2 concentrations being higher than the observations at this site with both models
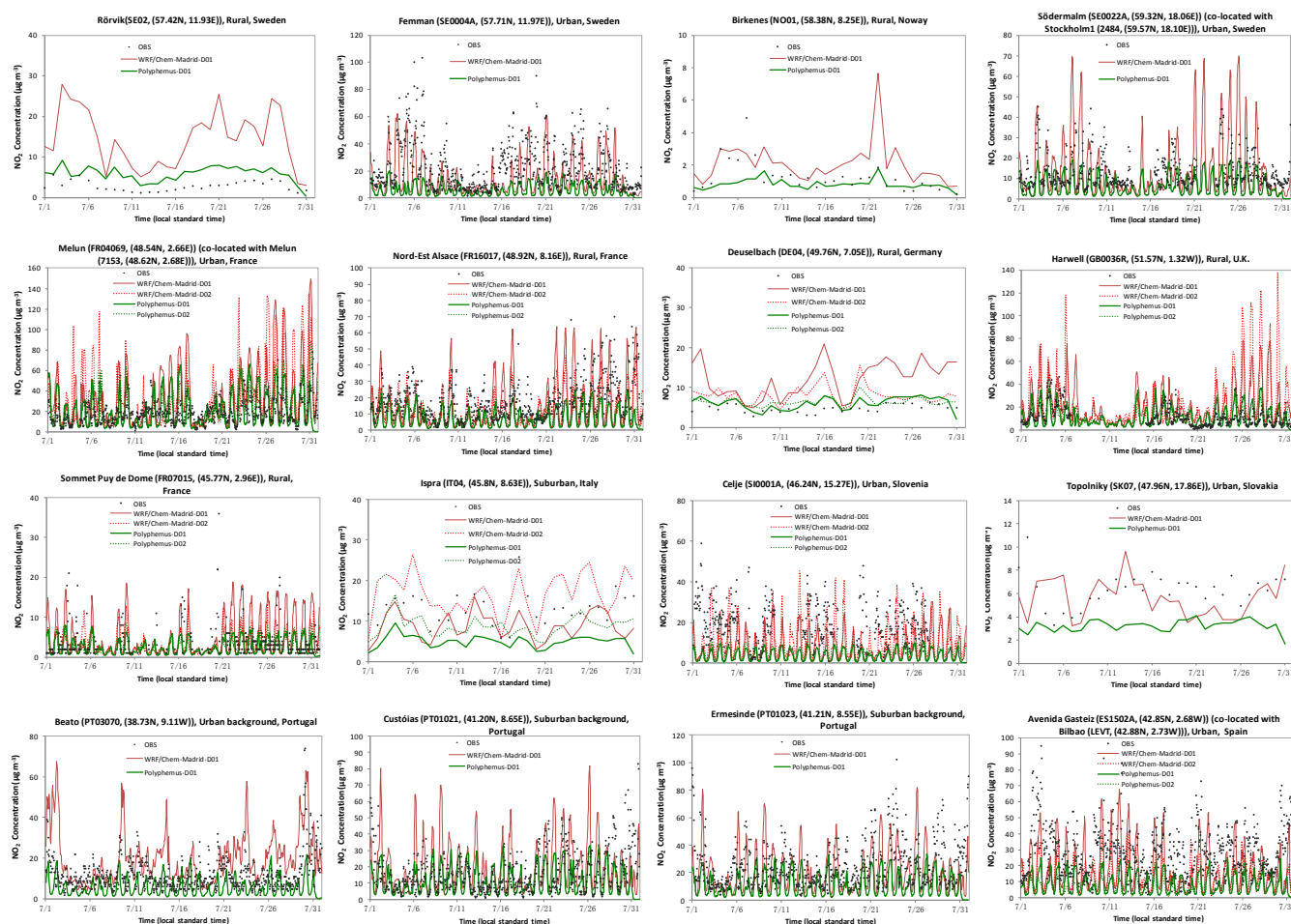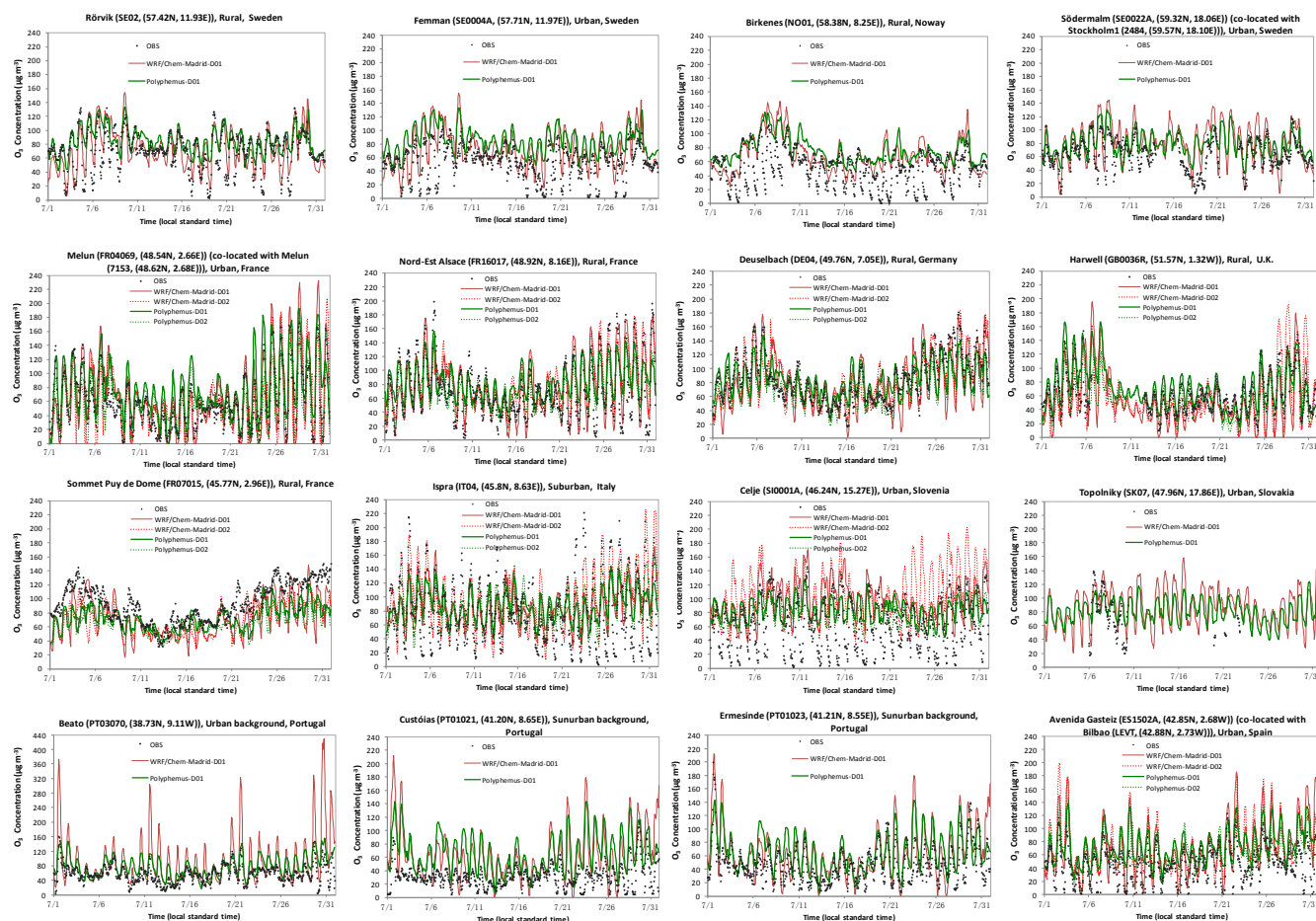
Fig. 4. Simulated and observed hourly or daily concentrations of NO_2 in July 2001 at selected sites over D01 and D02 in four latitude bands: 57–60° N, 48–52° N, 45–48° N, and 38–43° N (rows 1, 2, 3, and 4, respectively).

due to insufficient conversion of SO_2 to sulfate through gas-phase oxidation. At the suburban background site Custóias in Portugal, both models fail to reproduce the extremely high observed concentrations (mostly $>10\,\mu g\,m^{-3}$ and can reach as high as $210\,\mu g\,m^{-3}$). Custóias is located in the Greater Porto area, the second-largest city in northwestern Portugal where the pollutant emissions from its urban and industrial areas are among the highest in Portugal with the major pollution sources from road transport and other combustion processes (Ribeiro et al., 2012). The Porto area features a Mediterranean climate, with warm, dry summers and mild, rainy winters, which favors pollution buildup. At the suburban background site Ermesinde, located ~9 km northeast of Porto in Portugal, the observed SO_2 concentrations are available during 1–14 July and are much lower than those at Custóias. Both models give higher SO_2 concentrations in the second half of the month, although no observations are available for comparison.

Figure 4 shows the simulated and observed concentrations of hourly NO_2 at the 16 selected sites. In the north-

ern latitude band (57–60° N), at the 2 urban sites in Sweden (Femman and Södermalm), the observed NO_2 concentrations are very high, with monthly mean values of 21.4 and $12.7\,\mu g\,m^{-3}$ and peak values of 103 and $45\,\mu g\,m^{-3}$, respectively. The high NO_2 concentrations at Femman and Gothenburg are due partly to high NO_2 emissions from local vehicles and ships and partly to meteorological factors that lead to reduced local dispersion due to special topography (Haeger-Eugensson et al., 2010). Many streets at and near Södermalm in central Stockholm have very high levels of air pollutants due to high emissions of CO, NO_x, VOCs, and PM_{10} from road traffic (SLB-analys, 2006); additional NO_2 results from local photochemical reactions (Johansson and Forsberg, 2005), as well as unfavorable weather conditions for dispersion. While WRF/Polyphemus significantly underpredicts observed high NO_2 concentrations at both sites, WRF/Chem-MADRID shows much better agreement, although it underpredicts NO_2 concentrations that are greater than $60\,\mu g\,m^{-3}$ during 5–6 and 20 July at Femman and overpredicts peak NO_2 concentrations on some days

Fig. 5. Simulated and observed concentrations of hourly O_3 in July 2001 at selected sites over D01 and D02 in four latitude bands: 57–60° N, 48–52° N, 45–48° N, and 38–43° N (rows 1, 2, 3, and 4, respectively).

(e.g., 7–8, 21–22, 25–26 July). As discussed above, the discrepancies between simulated and observed NO_2 concentrations by both models at Södermalm and Femman are most likely caused by underestimation of emissions in the EMEP inventories, rather than biases in the meteorological predictions. At the 2 rural sites Rörvik, Sweden, and Birkenes, Norway, the observed NO_2 concentrations are much lower, with monthly mean values of 2.8 and 1.3 µg m^{-3} and peak values of 5.6 and 4.9 µg m^{-3}, respectively. Both models overpredict at Rörvik, with much larger overpredictions by WRF/Chem-MADRID. At Birkenes, WRF/Polyphemus simulates NO_2 well on most days with underpredictions during 5–7 July. While WRF/Chem-MADRID better simulates the observed NO_2 levels during 5–6 July, it still underpredicts those on 7 July, and overpredicts significantly those during 19–24 July. In the central latitude band (48–52° N), the observed NO_2 concentrations are typically > 10 µg m^{-3} and can be over 70 µg m^{-3} at the urban site Melun and the rural site Nord-Est Alsace in France. However, those are typically between 3 and 40 µg m^{-3} at Harwell, UK, and between 3 and 7 µg m^{-3} at Deuselbach, Germany. The major NO_2 sources

in Paris and at Harwell in southern UK are traffic emissions (Aphesis, 2002). While WRF/Polyphemus simulates NO_2 concentrations well at Melun and Harwell, WRF/Chem-MADRID significantly overpredicts them. Despite large underpredictions in 10 m wind speeds at Melun, the good performance in NO_2 predictions by WRF/Polyphemus but large overpredictions by WRF/Chem-MADRID indicate that biases in meteorological predictions are not a major factor explaining the different performance by the two models. Other factors such as differences in dry and wet deposition treatments and vertical distributions of emissions may explain most differences in the predictions by the two models. At Deuselbach, WRF/Polyphemus underpredicts on most days, and WRF/Chem-MADRID captures the magnitudes better on some days, despite underpredictions on some days. At Nord-Est Alsace, the NO_2 concentrations are underpredicted by WRF/Polyphemus and are generally well reproduced by WRF/Chem-MADRID. Nord-Est Alsace is located in Alsace, which is one of most industrialized regions in France, known for its hop harvesting and brewing, automobile industry, and phosphate mining. It is also one of the main

routes between France and Germany. This area thus has high NO_2 emissions from road traffic and various industrial sources. In the central south latitude band (45–48° N), the observed NO_2 concentrations are high at the urban site Celje, Slovenia (1–59 µg m^{-3}, mostly >3 µg m^{-3}, a monthly average of 19.5 µg m^{-3}) due to high NO_2 emissions from industry, diesel vehicles, and residential combustions and the weather conditions that favor pollutant buildup. They are relatively low at the other 3 sites due to lower sources of NO_2, with 1–36, 6–26, and 3–11 µg m^{-3} and monthly-mean values of 3.7, 13.0, and 6.3 µg m^{-3}, respectively, at Sommet Puy-de-Dôme, France; Ispra, Italy; and Topolniky, Slovakia. WRF/Chem-MADRID reproduces the observed NO_2 concentrations at Celje and Sommet Puy-de-Dôme on most days and at Ispra and Topolniky on some days, despite some underpredictions on some days at those sites. WRF/Polyphemus significantly underpredicts observations at all these sites. In the southern latitude band (38–43° N), the observed NO_2 concentrations are above 10 µg m^{-3} during most hours at all sites; they are in the range of 3–102, 2–95, 1–83, and 2–74 µg m^{-3} with monthly-mean values of 24.1, 28.9, 16.3, and 11.8 µg m^{-3}, respectively, at Ermesinde, Portugal; Avenida Gasteiz, Spain; Custóias, Portugal; and Beato, Portugal. Many manufacturing companies have operations in the Gasteiz area (including automobiles, tires, games, cookies, pasta, and flour), producing large NO_2 emissions. Its mild, humid temperate climate with warm summers also favors the photochemistry, which further enhances the local NO_2 levels at Avenida Gasteiz. The 3 urban or suburban background sites are located in the largest and second largest cities (i.e., Lisbon and Porto) in Portugal and their vicinity, where vehicle exhausts from road traffic provide a significant source of CO, NO_x, and VOCs (Barros et al., 2003; Ribeiro et al., 2012). The Mediterranean climate in these areas, with warm or hot and dry summers, favors photochemistry, which further enhances the NO_2 levels via greater O_3 concentrations available for NO titration. At all these sites, WRF/Chem-MADRID gives better agreement with observations than WRF/Polyphemus, despite discrepancies on some days. While the underpredictions in peak 2 m temperatures may contribute to the underpredictions in peak NO_2 concentrations at this site by both models due to less photochemistry as a result of less solar radiation and lower emissions of biogenic volatile organic compounds (BVOCs), inaccurate emissions of NO_2 in the EMEP inventory may play a more important role in the biases in the NO_2 predictions.

Figures 5 and 6 show simulated and observed concentrations of hourly and maximum 8 h O_3, respectively, at the 16 selected sites. The European Union (EU) air quality standard for maximum 8 h O_3 is 120 µg m^{-3} (with 25 exceedances allowed per year). Some European countries also have a standard for maximum 1 h O_3. For example, the maximum 1 h O_3 standard of Italy is 180 µg m^{-3}. In the northern latitude band (57–60° N), the observed hourly O_3 concentrations at the 4 sites are similar in terms of magnitudes (up to 132 µg m^{-3}) and diurnal variations. The O_3 concentrations exhibit a strong diurnal variation with nighttime O_3 levels as low as 1–3 µg m^{-3} at these sites, particularly at Birkenes and Femman. The observed daily variation trends and magnitudes (up to 122 µg m^{-3}) in the maximum 8 h O_3 are also similar at those sites. Note that the observed high maximum 8 h O_3 concentration of 122 µg m^{-3} is above the EU standard for O_3. At the 2 urban sites Femman and Södermalm, local vehicles and ships are predominant sources of CO, NO_2, and VOCs, leading to high O_3 formation. While NO_2 concentrations at Rörvik and Birkenes are low, the O_3 concentrations are similar to those at the 2 urban sites, indicating other possible causes such as the long-range transport (LRT) O_3 and O_3 precursors such as NO_x and VOCs from other European countries such as the UK, Poland, Denmark, and Russia (Øystein et al., 1997). Tang et al. (2009) studied the correlation between synoptic circulation and surface O_3 concentrations in southern Sweden and found that 85.5 % of high O_3 episodes at Rörvik are associated with three circulation patterns including anticyclonic weather pattern and the directional flows from southeast/east and southwest/south. This indicates a very important role of LRT during high O_3 episodes in rural areas in Sweden and Norway. Due to high latitudes, the daytime hours are long (~18 h) in summer at all these locations, favoring the photochemical O_3 formation. The special topography and/or the stable, low wind meteorological conditions at some sites (e.g., Femman and Södermalm in Sweden) also facilitate the pollution buildup. Both models generally capture high O_3 concentrations and the day-to-day variations at these sites (except for slight overpredictions on some days). Both models show a good agreement with nighttime O_3 at Södermalm. In particular, WRF/Chem-MADRID predicts much higher NO_2 concentrations that are in much better agreement with observed nighttime O_3 concentrations, illustrating the role of NO_x titration in determining nighttime O_3 levels. Both models, however, fail to reproduce the low O_3 concentrations at night at Rörvik, Femman, and Birkenes for different reasons. At Femman, the underpredictions of NO_x by both models (see Fig. 4) may have led to an insufficient titration of O_3 at night. At Rörvik and Birkenes, where observed NO_x concentrations are low, the very low observed nighttime O_3 concentrations may be caused by several other mechanisms. For example, O_3 can be destroyed by hydroxyl, hydroperoxyl, or organic radicals (OH, HO_2, and RO_2) (note that RO_2 can be produced from VOCs transported into these areas) in low-NO_x conditions, dominating nighttime O_3 chemistry (Monks, 2005). Both sites are on the coast, where the concentrations of sea salt are high. Chlorine/bromine atoms (Cl and Br) may be produced from heterogeneous reactions of sea salt with acidic species such as H_2SO_4 and HNO_3 at night (Monk, 2005; Jacobson, 2012), which can then destroy nighttime O_3 efficiently. Neither model includes the heterogeneous reactions of sea salt, and both models may underpredict concentrations of VOCs and associated RO_2 radicals

at Rörvik and Birkenes, leading to insufficient nighttime destruction of O_3 at both sites. For maximum 8 h O_3, both models give better agreement than hourly O_3, illustrating the models' capability of capturing daytime high O_3.

In the central latitude band (48–52° N), the observed O_3 concentrations at the four sites are much higher than those in the northern latitude band due to higher emissions of NO_x or VOCs or both at Melun and Harwell, which are located in the two largest metropolitan areas with dense population in Western Europe (i.e., Paris and London), and at Nord-Est Alsace, which is located in an industrialized region, or due likely to the influence of LRT on O_3 levels at Deuselbach, where there is no significant local sources and emissions from polluted areas east and southeast of Deuselbach, such as Frankfurt (Andre et al., 1981). The observed hourly O_3 concentrations can reach up to $172\,\mu g\,m^{-3}$ at Melun, $199\,\mu g\,m^{-3}$ at Nord-Est Alsace, $181\,\mu g\,m^{-3}$ at Deuselbach, and $154\,\mu g\,m^{-3}$ at Harwell, close to or above the hourly O_3 standard of $180\,\mu g\,m^{-3}$ in some European countries. The observed maximum 8 h O_3 concentrations can reach up to $159\,\mu g\,m^{-3}$ at Melun, $176\,\mu g\,m^{-3}$ at Nord-Est Alsace, $170\,\mu g\,m^{-3}$ at Deuselbach, and $131\,\mu g\,m^{-3}$ at Harwell, all of which are well above the EU maximum 8 O_3 standard of $120\,\mu g\,m^{-3}$. The first and last weeks of July 2001 are high O_3 episodes in these areas. At these sites, WRF/Chem-MADRID reproduces both daytime and nighttime O_3 levels very well, despite some overpredictions of daytime peak O_3 due in part to overpredicted NO_2 concentrations and in part to biases in meteorological predictions (e.g., underpredicted 10 m wind speed at Melun) and despite underpredictions of nighttime low O_3 levels due to overpredicted titration of nighttime O_3 by NO_x during a few hours at some sites (e.g., 3–5 July at Melun and 26–31 July at Harwell). As shown in Fig. 13 in Part 1, wind speeds are significantly underpredicted at Melun, which may explain in part the overpredictions in the SO_2 concentrations at Melun due to underestimated dispersion. WRF/Polyphemus captures well the O_3 concentrations and diurnal variations at Melun and Harwell, but tends to underpredict the daytime peak O_3 levels and overpredict the nighttime low O_3 levels at Nord-Est Alsace and Deuselbach. Both models simulate maximum 8 h O_3 well on most days at Melun: WRF/Chem-MADRID gives better agreement than WRF/Polyphemus at Nord-Est Alsace and Deuselbach, and WRF/Polyphemus gives better agreement at Harwell.

In the central south latitude band (45–48° N), the observed hourly and maximum 8 h O_3 levels at Ispra are the highest among the four sites, reaching 252 and $197\,\mu g\,m^{-3}$, respectively, in late afternoon (15:00–16:00 local standard time), both of which exceeded the EU maximum 8 h standards and the hourly O_3 standards adopted in some European countries. This is because of the transport of O_3 and/or O_3 precursors from more polluted areas such as Milan to Ispra when mountain breeze develops in the afternoon and when the prevailing wind direction is from the south, where the urban and

the industrial areas are located (Perrino and Putaud, 2003). Exceedances of the maximum 8 h O_3 at other sites on some days also occurred on some days at other sites. The model performance varies strongly from site to site. At the rural site Sommet Puy-de-Dôme in France, while both models generally capture the day-to-day variation of hourly O_3 (e.g., relatively higher observed O_3 levels during 2–7 July and 22–31 July), WRF/Chem-MADRID shows better agreement in terms of amplitudes of daily variations and magnitudes of the peak O_3 concentrations. At the suburban site Ispra, Italy, WRF/Chem-MADRID gives better agreement with observed hourly O_3 than WRF/Polyphemus, although it still underpredicts peak O_3 on some days and overpredicts the minimal O_3 on most days. At the urban site Celje, Slovenia, WRF/Chem-MADRID overpredicts daytime O_3 levels, and WRF/Polyphemus gives better agreement. But both models fail to reproduce the nighttime O_3 levels due mainly to underpredictions in NO_x concentrations (see Fig. 4 for NO_2 predictions). At another urban site, Topolniky, in Slovakia, a comparison of very limited observational data on a few days shows reasonably good agreement by both models, with better agreement on observed peak O_3 concentrations on 6–7 July and minimal nighttime O_3 concentrations on 8–9 July by WRF/Chem-MADRID. The observed maximum 8 h O_3 levels are well reproduced but largely underpredicted by WRF/Polyphemus at Sommet Puy-de-Dôme and Ispra. At Celje and Topolniky, while WRF/Chem-MADRID better captures higher maximum 8 h O_3 values ($>100\,\mu g\,m^{-3}$) on some days, WRF/Polyphemus better captures moderate O_3 values (80–$100\,\mu g\,m^{-3}$) on some days, but neither reproduces lower maximum 8 h O_3 values ($<80\,\mu g\,m^{-3}$) at Celje due mainly to underpredictions of NO_x (thus insufficient titration of O_3) at this site.

In the southern latitude band (38–43° N), observed O_3 levels are overpredicted by both models with much closer agreement with observations by WRF/Polyphemus at the urban background site Beato, Portugal, and are significantly overpredicted by both models at Custóias in Portugal. Both models simulate hourly O_3 much better at Ermesinde in Portugal and Avenida Gasteiz in Spain in terms of both daily and hourly variations and magnitudes, despite overpredictions on some days by both models with greater overpredictions on more days by WRF/Chem-MADRID. For maximum 8 h O_3, large overpredictions occur on most days at all sites, in particular, by WRF/Chem-MADRID at Beato and Avenida Gasteiz and by both models at Custóias and Ermesinde.

Figure 7 shows simulated and observed hourly concentrations of $PM_{2.5}$ and PM_{10} at four sites where hourly data are available. At Kallio, an urban background site in Helsinki, the capital of Finland, the observed $PM_{2.5}$ and PM_{10} concentrations are 9.9 and $20.4\,\mu g\,m^{-3}$ for monthly average and can be up to 35.5 and $369.2\,\mu g\,m^{-3}$, respectively. Anthropogenic emissions of $PM_{2.5}$ and their gaseous precursors in Finland are low compared to the more polluted regions in Europe (EMEP, 2006a, b). A total of 50–70 % of
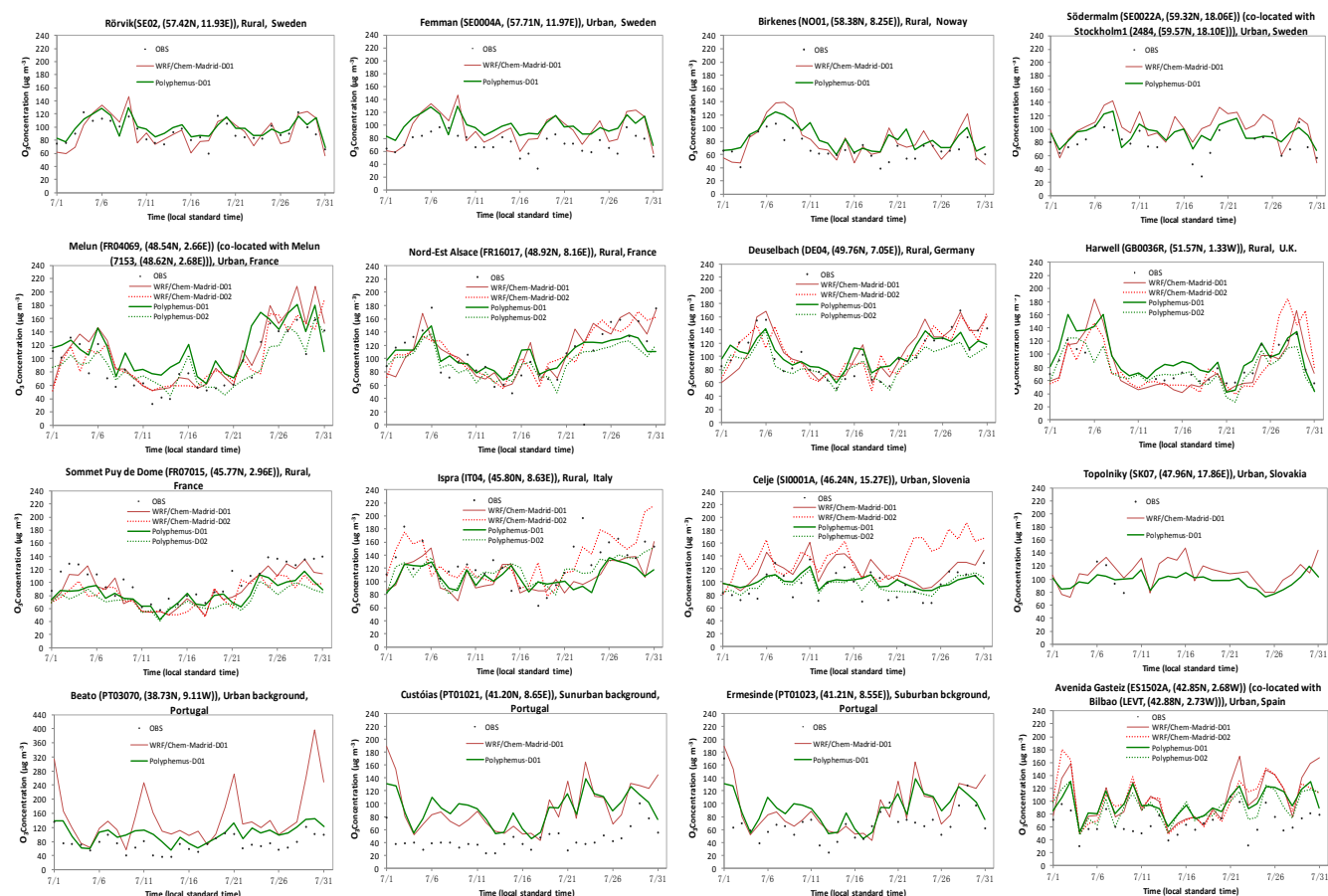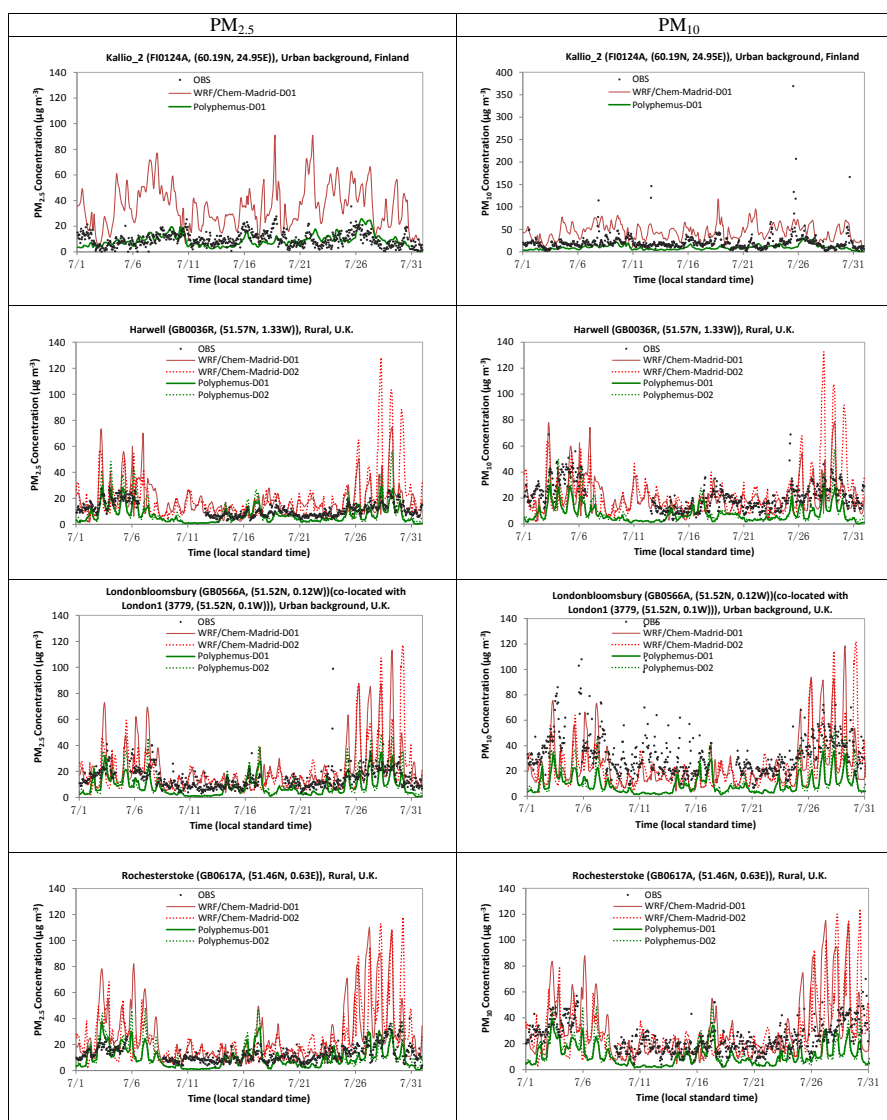
Fig. 6. Simulated and observed concentrations of max 8 h O_3 in July 2001 at selected sites over D01 and D02 in four latitude bands: 57–60° N, 48–52° N, 45–48° N, and 38–43° N (rows 1, 2, 3, and 4, respectively).

the $PM_{2.5}$ mass in the urban areas in Helsinki originates from the LRT of high PM concentrations from several countries such as Estonia, Latvia, Lithuania, Russia, Belarus, Ukraine, and/or Poland, where pollutant emissions from various sources (e.g., energy production, traffic, industry, residential burning, and open biomass burning) are high (Vallius et al., 2003; Karppinen et al., 2004; Sogacheva et al., 2005; Kauhaniemi et al., 2007; van Aardenne et al., 2007). However, the extremely high PM_{10} concentrations observed on July 25 at this site are most likely due to the resuspension of road dust particles, because road dust is a significant source of mineral particles in urban areas of Finland (Pakkanen et al., 2001; Kupiainen and Tervahattu, 2004; Putaud et al., 2004; Tervahattu et al., 2006; Anttila and Salmi, 2006). WRF/Polyphemus generally reproduces hourly $PM_{2.5}$ concentrations well, whereas WRF/Chem-MADRID significantly overpredicts it due likely to several factors. First, the concentrations of gaseous precursors of secondary $PM_{2.5}$ (e.g., SO_4^{2-}, NH_4^+, and NO_3^-) such as SO_2, NH_3, and HNO_3 and primary PM species are overpredicted due to lower heights of first model layers for some grid cells and thinner

thickness of the model layer and the use of lower dry deposition velocities of the gas precursors as described in the Part 1 paper. Second, the dry deposition velocities of $PM_{2.5}$ species calculated in WRF/Chem-MADRID may also be lower than those of WRF/Polyphemus. Third, the wet scavenging rates calculated in WRF/Chem-MADRID may be lower than those in WRF/Polyphemus. The observed hourly PM_{10} concentrations are significantly underpredicted by WRF/Polyphemus due to neglect of road dust emissions in the EMEP inventories and much better reproduced by WRF/Chem-MADRID due to inclusion of online soil dust emissions and higher seasalt concentrations even though underpredictions remain on most days. Neither model reproduces several extremely high PM_{10} episodes ($>100 \, \mu g \, m^{-3}$) during 7, 12, 25, and 30 July due to missing road dust emissions in the EMEP inventories.

The main sources of PM_{10} in the UK in 2001 include road transport emissions (in particular, exhaust gases from diesel engines), other sectors such as solvent processes, agriculture, and waste treatment, industrial processes (e.g., the production of metals, cement, lime, coke and chemicals, bulk handling of dusty materials, construction, mining and
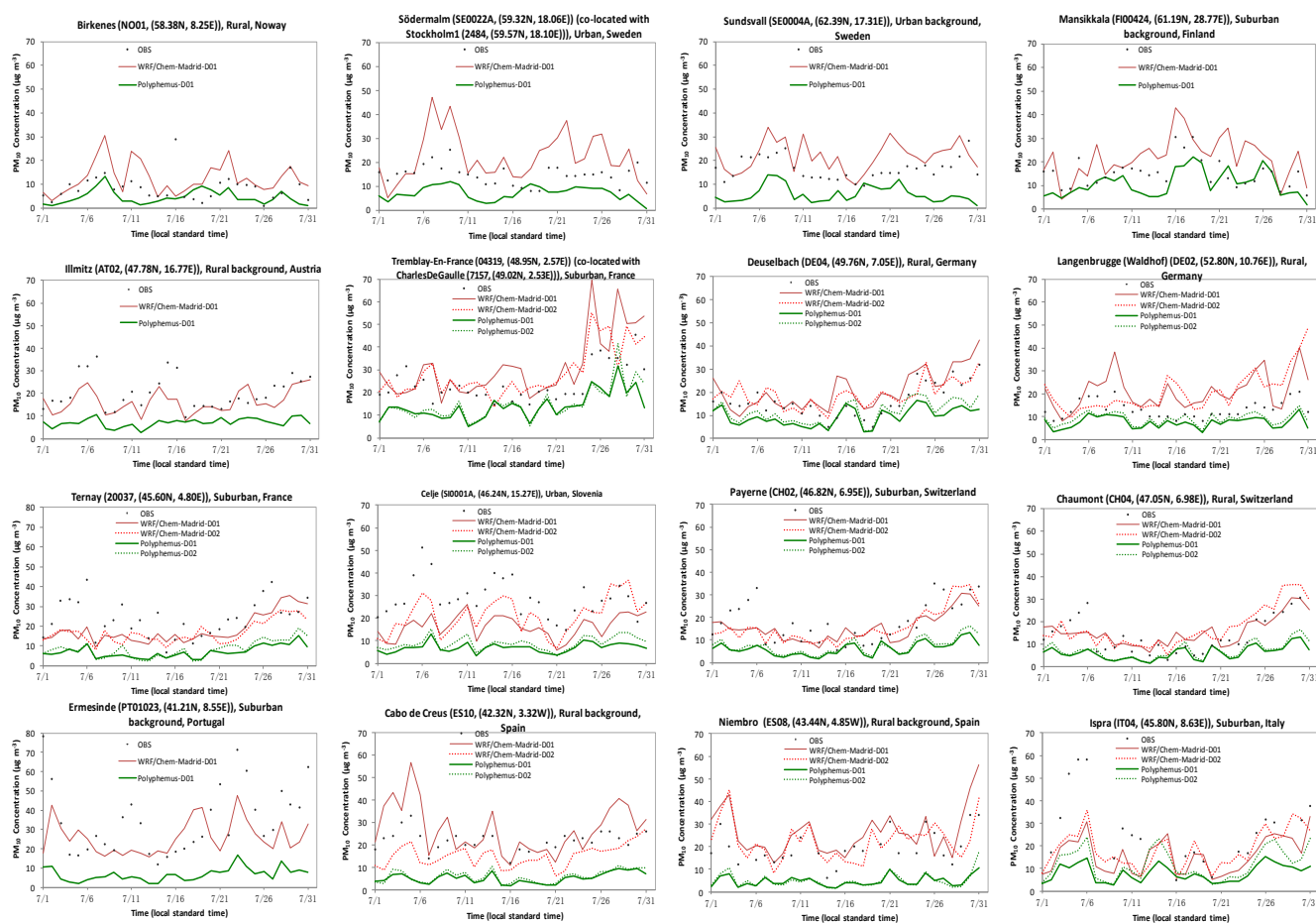
Fig. 7. Simulated and observed hourly concentrations of PM$_{2.5}$ and PM$_{10}$ in July 2001 at selected sites over D01 and D02.

quarrying), commercial, domestic and agricultural combustion (e.g., mainly of coal and solid fuels), industrial combustion, and energy industries (i.e., power generation) (MacCarthy et al., 2012). Observed and simulated PM$_{2.5}$ and PM$_{10}$ concentrations at three sites are shown in Fig. 7. The urban background site London Bloomsbury, located in central London, is surrounded by a busy two-lane, one-way road system and subject to frequent congestion. It has the highest PM$_{2.5}$ and PM$_{10}$ concentrations among the three sites in the UK. The observed PM$_{2.5}$ and PM$_{10}$ concentrations at this site are 14.5 and 32.9 μg m^{-3} for monthly average and can be up to 99 and 137 μg m^{-3}, respectively. WRF/Polyphemus generally reproduces hourly PM$_{2.5}$ concentrations in terms of daily variations and magnitudes, whereas WRF/Chem-MADRID significantly overpredicts the concentrations in

early and late July. Despite underpredictions in the first half of July and overpredictions in late July, WRF/Chem-MADRID gives much higher PM$_{10}$ concentrations and thus better agreement with observations than WRF/Polyphemus due mainly to the inclusion of online road dust emissions. As shown in Fig. 12 in Part 1, WRF largely underpredicts 10 m wind speed at London, which may contribute in part to the overpredictions in PM$_{2.5}$ and PM$_{10}$ concentrations at this site. At the rural site Rochester Stoke, located in the city of Rochester about 48 km from London in the southeastern corner of England, WRF/Polyphemus generally captures the daily variations and magnitudes of the hourly PM$_{2.5}$ concentrations, whereas WRF/Chem-MADRID significantly overpredicts them. Despite large underpredictions in early and late July, WRF/Chem-MADRID gives better agreement for
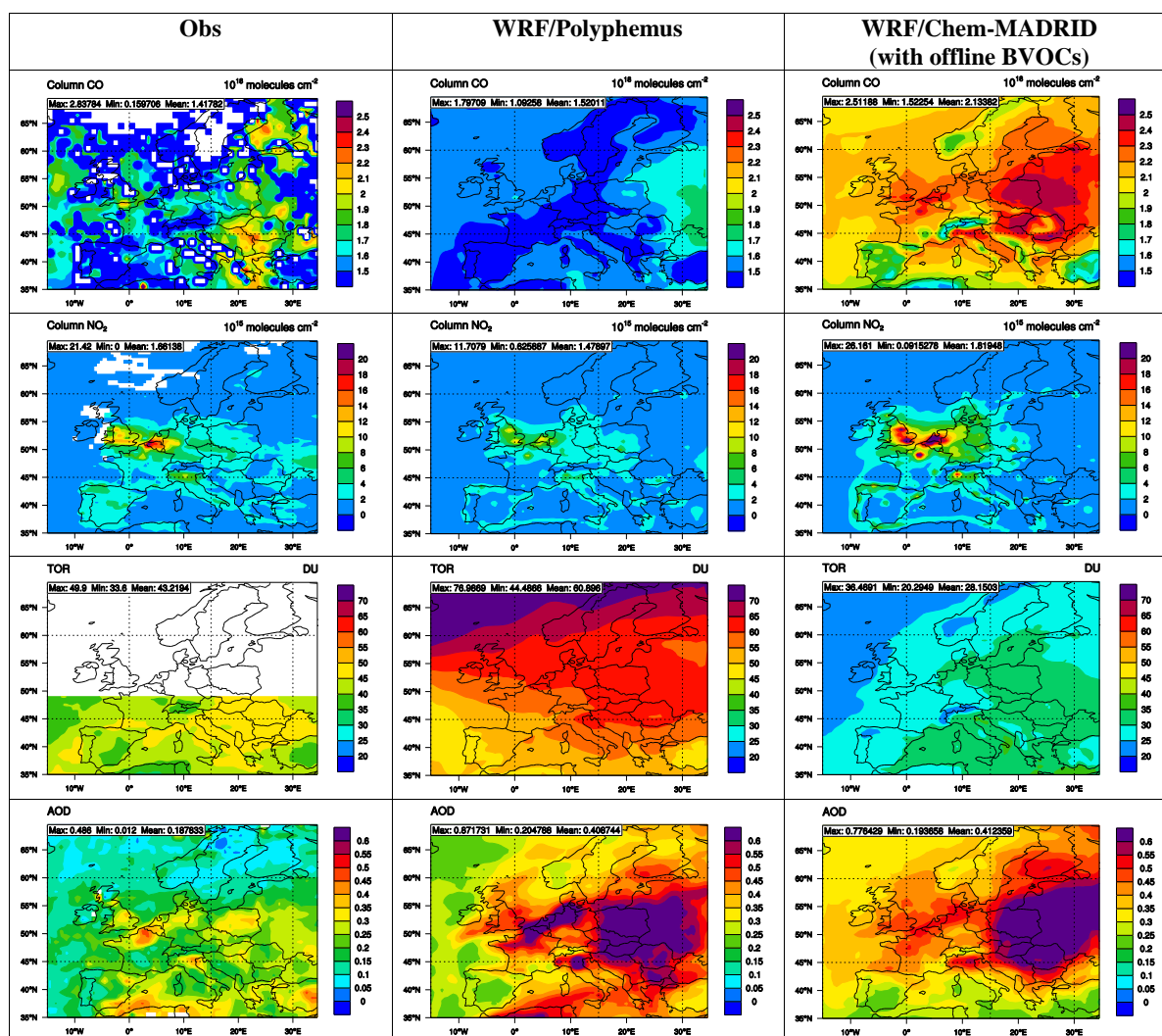
Fig. 8. Simulated and observed concentrations of 24 h average PM_{10} at July 2001 selected sites over D01 and D02 in four latitude bands: 57–60° N, 48–52° N, 45–48° N, and 38–43° N (rows 1, 2, 3, and 4, respectively).

hourly PM_{10} concentrations in terms of both daily variations and magnitudes, compared to WRF/Polyphemus, which significantly underpredicts PM_{10} concentrations on most days. At the rural site Harwell, UK, WRF/Chem-MADRID significantly overpredicts the concentrations of $PM_{2.5}$, and WRF/Polyphemus simulates them well. WRF/Polyphemus tends to underpredict hourly PM_{10} concentrations on most days; on the other hand, WRF/Chem-MADRID gives better agreement on most days except for 26 and 28–30 July.

Figure 8 shows simulated and observed 24 h average concentrations of PM_{10} at the 16 sites. In the northern latitude band (57–60° N), among the 4 sites, the observed PM_{10} concentrations are the highest at Mansikkala, with a monthly observed mean concentration of $15.2 \, \mu g \, m^{-3}$ and the peak daily concentration of $30.6 \, \mu g \, m^{-3}$. Mansikkala is a suburban background located in Imatra, an industrial and coastal town in southern Finland, where the PM_{10} concentrations are affected by local sources, LRT of PM_{10} from Eastern European countries, and sea-salt emissions. The observed PM_{10} concentrations are also high at Södermalm, an urban site, located in central Stockholm on the south-

central east coast of Sweden and Sundsvall, an urban background site on the east coast and middle portion of Sweden, with monthly observed mean concentrations of 14.8 and $16.5 \, \mu g \, m^{-3}$ and the peak daily concentrations of 25.2 and $28.2 \, \mu g \, m^{-3}$, respectively. Stockholm air is dirtier than that of Los Angeles, according to the most recent report from the World Health Organization (WHO) (http://www.who.int/phe/health_topics/outdoorair/databases/en/index.html). Road traffic is the most important source of particles in Stockholm's inner city; in particular, vehicle exhaust emissions produce ultrafine particles as a result of imperfect combustion of diesel and petrol (Johansson et al., 2004, 2007; Norman and Johansson, 2006). The observed PM_{10} concentrations are relatively low at Birkenes, a rural, coastal site ~30 km from Kristiansand in southern Norway with a monthly observed mean concentration of $8.4 \, \mu g \, m^{-3}$ and the peak daily concentration of $28.9 \, \mu g \, m^{-3}$. WRF/Polyphemus underpredicts PM_{10} concentrations at all sites, whereas WRF/Chem-MADRID overpredicts them, in particular, at Södermalm. Such differences may be attributed to a different emission module of sea salt with higher sea-salt emissions

Fig. 9. Simulated and observed monthly mean column mass abundance of CO and NO$_2$, tropospheric ozone residual (TOR), and aerosol optical depth (AOD) over D01.

from WRF/Chem-MADRID and the inclusion of emissions of soil dust.

In the central latitude band (48–52° N), the observed PM$_{10}$ concentrations are higher at Illmitz, Tremblay-en-France, and Deuselbach than at sites in Nordic Europe, with monthly observed mean concentrations of 20.3, 23.9, and 16.4 µg m^{-3} and the peak daily concentrations of 36.3, 45.5 and 32.0 µg m^{-3}, respectively. Illmitz is a rural background site located in the Neusiedler See-Seewinkel National Park on the eastern shore of Lake Neusiedl in eastern Austria. The area has wide open plains and salt marsh flora, with many small salt lakes around. The observed higher PM$_{10}$ concentrations indicate the influence of LRT of polluted air mass with high PM$_{2.5}$ concentrations. Based on the wind direction analysis of Barmpadimos et al. (2012), the high PM concentrations are more associated with the east wind direction as compared to the west wind direction, indicating

that the sources of high PM$_{10}$ concentrations most likely originated from Eastern Europe rather than Western Europe because of their higher levels of air pollution. Tremblay-en-France is a suburban site in the northeastern suburbs of Paris ($\sim$19.5 km from Paris). The high PM concentrations at this site may be caused by local road vehicles. Deuselbach is a rural site located $\sim$150 km southwest of Cologne in southwestern Germany. The high PM concentrations at this site may be caused by LRT of PM$_{10}$ concentrations from Cologne. The observed PM concentrations are relatively low at Langenbrugge, with a monthly observed mean concentration of 13.2 µg m^{-3} and the peak daily concentration of 21.0 µg m^{-3}. WRF/Polyphemus significantly underpredicts observed PM$_{10}$ concentrations on most days at all sites. WRF/Chem-MADRID captures them on most days except for underpredictions of high PM$_{10}$ concentrations ($>$25 µg m^{-3}) on a few days at Illmitz and overpredictions

of high PM_{10} concentrations ($>30 \,\mu g \,m^{-3}$) on a few days at Tremblay-En-France. It overpredicts observed PM_{10} concentrations on most days at Deuselbach and Langenbrugge. As shown in Fig. 12 in Part 1, WRF underpredicts in 10 m wind speeds at Tremblay-en-France, which may contribute in part the overpredictions in PM_{10} concentration at this site.

In the central south latitude band (45–48° N), the observed PM_{10} concentrations are also high due to high precursor levels and the favorable weather conditions for PM formation and transport. The monthly observed mean concentrations are 23.9, 28.7, 17.9, and 13.9 $\mu g \,m^{-3}$ and the peak daily concentrations are 43.5, 51.1, 34.9, and 30.6 $\mu g \,m^{-3}$ at Ternay, Celje, Payerne, and Chaumont, respectively. Ternay is a suburban site located ∼18 km south of Lyon, a large city in southeastern France. Traffic emissions are a major contributor to the concentrations of $PM_{2.5}$ in this region. Major sources of PM_{10} include agriculture and forestry, the manufacturing industry (e.g., the Feyzin refinery), the residential/tertiary sector and road transport (http://www. eea.europa.eu/soer/countries/fr). The high level of PM_{10} at Celje, an urban site, in Slovenia has been a great concern (Otorepec and Gale, 2004). The main sources of PM_{10} pollution are industry and traffic, including both transit and diesel buses. Payerne is a suburban mountain site located in the Swiss Plateau and surrounded by the Alps on the east and the Jura Mountains on the west in western Switzerland. A total of 59.8 % of its land is used for agricultural purposes. Chaumont is a rural site on the mountain Chaumont in the city of Neuchâtel in western Switzerland. Renowned for its watch industry, Neuchâtel is the heart of micro-technology and high-tech industry. The major PM_{10} sources in Switzerland include agriculture/forestry, industry, transport, and households (http://www.eea.europa.eu/soer/ countries/ch). While WRF/Polyphemus significantly underpredicts observed PM_{10} concentrations on nearly all days at all sites, WRF/Chem-MADRID gives better agreement at all sites, in particular, Chaumont.

In the southern latitude band (38–43° N), the observed PM_{10} concentrations remain high at all sites, with monthly observed mean concentrations of 34.8, 22.1, 19.4, and 26.4 $\mu g \,m^{-3}$ and the peak daily concentrations of 78.3, 33.0, 34.0, and 58.2 $\mu g \,m^{-3}$ at Ermesinde, Cabo de Creus, Niembro, and Ispra, respectively. Ermesinde is a suburban background site in the Porto area, where air pollutant emissions are among the largest in Portugal. In addition to domestic sources such as vehicle exhausts from road traffic, suspended road dust, and industry combustions, average daily PM_{10} concentrations in Portugal can be caused partly by LRT of particles from natural events, particularly from the Sahara desert or forest fires (http://www.eea. europa.eu/soer/countries/pt/). Cabo de Creus is a rural background site in the Cap de Creus peninsula on the easternmost point of mainland Catalonia in Spain, ∼25 km south of the French border. The peninsula is a natural park and very rocky dry region, with almost no trees. The Girona

area acts as an industrial, commercial and service hub for a significant part of the province, producing high emissions of air pollutants including PM_{10}. Niembro is a rural background, beach site in the province of Asturias in northern Spain. The major sources of air pollutants in Spain include energy processing (including transport), agriculture, industrial processes, waste treatment and disposal, and solvent use (http://www.eea.europa.eu/soer/countries/es). In addition to the aforementioned emission sources, the resuspended particles from paved roads are an important contributor to PM_{10} and strongly affect local coarse PM concentrations at both sites (Pay et al., 2011). Ispra is a suburban site in Italy, where transportation (in particular, the roadway transportation) is the main source of PM_{10} pollution, followed by industry, the residential combustion, and agriculture (http://www.eea. europa.eu/soer/countries/it). While WRF/Polyphemus simulates well the observed $PM_{2.5}$ concentrations, it significantly underpredicts the observed PM_{10} concentrations at all sites. On the other hand, WRF/Chem-MADRID tends to overpredict the observed $PM_{2.5}$ concentrations, but it gives much better agreement for the observed PM_{10} concentrations probably because of the overprediction of $PM_{2.5}$ concentrations and because of the inclusion of mineral dust emissions through the use of the online dust emission module and the impact of Saharan dust emissions through boundary conditions, as well as higher sea-salt emissions.

3.2   Evaluation of column variables

Figure 9 shows simulated and observed monthly-mean column variables over D01. The corresponding domainwide performance statistics is shown in Table 1. WRF/Polyphemus gives relatively good performance for column CO and NO_2 mass concentrations in terms of domainwide statistics, but it gives a very low correlation coefficient for column CO and fails to reproduce high observed column CO concentrations in most of the domain. WRF/Chem-MADRID significantly overpredicts column CO and NO_2 mass concentrations, but gives better correlation for column CO and better captures high column CO and NO_2 mass concentrations. The large differences between the column CO concentrations predicted by the two models are likely caused by differences in the boundary conditions and in the dry position velocity of CO, with higher boundary conditions (by 1.5–39.4 % in layers 6–22) and lower dry position velocity by WRF/Chem-MADRID, leading to higher column CO concentrations. The use of a different number of layers in both models (23 layers in WRF/Chem-MADRID and 22 layers in WRF/Polyphemus) also explains some of the differences in CO. The large differences between the column NO_2 concentrations predicted by the two models are likely caused by differences in vertical distributions of NO_x emissions and the dry deposition velocity of NO_2 (with lower values by WRF/Chem-MADRID, leading to higher column NO_2 concentrations). WRF/Polyphemus moderately

overpredicts the tropospheric ozone residual (TOR) with an NMB of 26.8 %, whereas WRF/Chem-MADRID moderately underpredicts TOR with an NMB of -30.6 %. Neither captures the observed magnitudes of TOR, with better gradients by WRF/Polyphemus and better correlation by WRF/Chem-MADRID. Despite higher surface O_3 concentrations by WRF/Chem-MADRID, WRF/Chem-MADRID gives much higher TOR than WRF/Polyphemus. This indicates that the large differences between TOR concentrations predicted by the two models are caused by different boundary conditions for O_3 used in the two model simulations, which are ~47 and 78 $\mu g\,m^{-3}$ for layers 1–19 and ~26 and 121 $\mu g\,m^{-3}$ for layers above 19 for WRF/Chem-MADRID and WRF/Polyphemus, respectively. The values used in WRF/Chem-MADRID are lower by 33.5–82 % than those used in WRF/Polyphemus, leading to a much lower TOR. Aerosol optical depth (AOD) is calculated in a post-processing step at 600 nm, as detailed in Tombette et al. (2008). The aerosol complex refractive index is computed by assuming that black carbon is not internally mixed with other PM species (i.e., having a core/shell structure). The wet diameter is deduced from the dry diameter and the liquid water content obtained from ISORROPIA. In WRF/Chem, AOD is calculated at 550 nm using the parameterization of Ghan et al. (2001), which performs full Mie calculations to calculate aerosol scattering and absorption coefficients as a function of PM number concentrations, single-particle radius, and single-particle absorption and scattering efficiencies over a set of seven complex refractive indices that represent a range of indices typical of atmospheric aerosols, as described in Fast et al. (2005). Both models significantly overpredict AOD with NMBs of 125 % and 129.6 %, respectively, but WRF/Polyphemus shows better correlation for AOD. These AOD overpredictions confirm the hypothesis that underpredictions of PM at individual sites (mostly urban) result mostly from underestimation of local emission inventories (e.g., road dust) or misrepresentation of pollutant vertical distribution rather than regional biases. Similar to column CO and NO_2 predictions, WRF/Chem-MADRID gives higher AOD than WRF/Polyphemus due to aforementioned differences in the model treatments of vertical structures, dry and wet deposition, boundary conditions, and aerosol thermodynamics and dynamics.

4 Sensitivity simulations

4.1 Sensitivity to horizontal grid resolutions

Figures 1 and 2 show simulated spatial distributions of SO_2, NO_2, maximum 8 h O_3, and 24 h average $PM_{2.5}$, PM_{10}, and PM_{10} composition by the two models overlaid with observations over D02 in July. Compared to spatial distributions over D01, the simulations over D02 by both models show greater details in hot spots or areas with lower con-

centrations for all species, particularly for NO_2, maximum 8 h O_3, $PM_{2.5}$, NH_4^+, NO_3^-, and TOM. Figures 3–6 compare observed and simulated hourly concentrations of SO_2, NO_2, and O_3 and maximum 8 h O_3, respectively, from the simulations at horizontal grid resolutions of 0.5° over D01 and 0.125° over D02 at 8 sites that fall into the D02 domain. For SO_2, WRF/Polyphemus predictions at the two grid resolutions are overall similar at Melun, Nord-Est Alsace, and Sommet Puy-de-Dôme, France, where the terrain is either low or uniform but different at mountain/high altitude sites or sites with complex terrain (i.e., Deuselbach, Germany; Harwell, UK; Ispra, Italy; Celje, Slovenia; and Avenida Gasteiz, Spain). WRF/Chem-MADRID also gives similar results at the two grid resolutions at Nord-Est Alsace and Sommet Puy-de-Dôme, France, but shows high sensitivity to grid resolutions at remaining sites. Both models give higher values at 0.125° over D02, leading to an overall better agreement at most sites except for Deuselbach, Harwell, and Ispra, where the overpredictions are greater. For NO_2, WRF/Polyphemus predictions at the two grid resolutions are quite similar at all sites except for Ispra, where the use of a finer grid resolution brings predictions into a better agreement with observations. WRF/Chem-MADRID shows a high sensitivity to grid resolutions at all sites, with better agreement at Nord-Est Alsace and Celje, but worse agreement at Melun, Sommet Puy-de-Dôme, Deuselbach, Harwell, Ispra, and Avenida Gasteiz. For hourly O_3, WRF/Polyphemus at both grid resolutions gives similar predictions but with lower nighttime O_3 values at a finer grid resolution at all sites, leading to a closer agreement with observations. WRF/Chem-MADRID gives higher daytime peak values but lower nighttime values at all sites, leading to an overall better agreement with observations at all sites expect for Celje. For maximum 8 h O_3, WRF/Polyphemus at 0.125° gives lower values than at 0.5° on most days at all sites except for Ispra, leading to better agreement with observations. WRF/Chem-MADRID shows a higher sensitivity to grid resolutions than WRF/Polyphemus, but the values at 0.125° could be either higher or lower than those at 0.5°, depending on the sites. This leads to a better agreement with observations at Melun, Nord-Est Alsace, Ispra, and Avenida Gasteiz, but worse agreement at Deuselbach, Sommet Puy-de-Dôme, Harwell, and Celje.

Figures 7–8 compare observed and simulated hourly $PM_{2.5}$ and PM_{10} concentrations at 3 sites and 24 h average concentrations of PM_{10} at 10 sites that fall into the D02 domain (i.e., Tremblay-en-France and Ternay, France; Deuselbach and Langenbrugge, Germany; Payerne and Chaumont, Switzerland; Ispra, Italy; Celje, Slovenia; Harwell, Rochester Stoke, and London Bloomsbury, UK; and Cabo de Creus and Niembro, Spain). For hourly $PM_{2.5}$ and PM_{10}, WRF/Polyphemus shows less sensitivity to grid resolutions than WRF/Chem-MADRID at Harwell, Rochester Stoke, and London Bloomsbury, with better agreement with observations. WRF/Chem-MADRID at 0.125° gives higher

Table 2. Comparison of performance statistics of WRF/Polyphemus and WRF/Chem-MADRID over D02.[1]

Variable	Network	Data Pair[2]	Mean Obs[3]	Mean Mod[3,4,5] D01 in D02 WP	WC-S	D02 WP	WC-S	Corr[4] D01 in D02 WP	WC-S	D02 WP	WC-S	MB[3,5] D01 in D02 WP	WC-S	D02 WP	WC-S	RMSE[3,5] D01 in D02 WP	WC-S	D02 WP	WC-S	NMB[5] (%) D01 in D02 WP	WC-S	D02 WP	WC-S	NME[5] (%) D01 in D02 WP	WC-S	D02 WP	WC-S
Hourly NH_3	AIRBASE	3223	11.0	8.7	9.0	9.3	9.1	0.3	0.4	0.4	0.3	−2.3	−2.0	−1.7	−1.9	14.0	15.5	14.1	15.9	−21.1	−18.4	−15.3	−16.8	79.5	83.5	79.8	85.3
Daily NH_3	EMEP	51	9.3	7.8	8.6	8.9	8.8	0.7	0.7	0.9	0.7	−1.5	−0.7	−0.4	−0.5	4.5	7.7	4.5	5.6	−16.1	−8.0	−4.8	−5.2	36.5	56.8	31.2	37.9
Daily HNO_3	EMEP	31	1.0	2.9	4.0	3.5	4.5	0.3	0.3	0.4	−0.1	1.9	3.0	2.6	3.5	2.1	3.6	2.8	4.3	193.6	305.0	259.2	354.9	314.0	259.2	361.6	216.3
Hourly SO_2	AIRBASE	473915	4.9	3.5	5.8	3.8	5.9	0.2	0.2	0.2	0.2	−1.4	0.9	−1.1	1.0	9.1	9.8	9.2	10.2	−28.4	19.2	−22.4	21.3	72.8	76.8	70.7	99.7
Daily SO_2	BDQA	685	5.3	3.4	5.6	3.8	5.2	0.5	0.5	0.5	0.2	−1.9	0.3	−1.4	0.0	10.2	10.9	10.3	10.9	−36.1	6.4	−26.9	−0.9	85.5	98.9	85.5	96.8
Daily SO_2	EMEP	31	1.1	2.5	4.1	2.4	3.7	0.5	0.5	0.5	0.2	1.4	3.0	1.3	2.6	2.1	4.4	2.2	3.5	126.1	270.4	121.9	230.1	137.0	275.5	137.6	234.9
Hourly NO_2	AIRBASE	619916	18.0	8.1	15.6	8.4	15.8	0.5	0.3	0.5	0.3	−9.9	−2.4	−8.7	−2.2	18.6	19.4	17.5	19.7	−55.0	−13.5	−48.5	−12.2	69.9	72.4	67.5	72.8
Hourly NO_2	BDQA	55326	16.0	7.2	13.5	6.5	12.1	0.3	0.2	0.3	0.3	−8.8	−2.5	−7.6	−3.8	17.5	12.8	17.3	17.9	−54.7	−15.4	−47.4	−23.9	75.3	81.9	74.1	75.0
Daily NO_2	EMEP	483	6.5	6.2	12.5	6.5	12.0	0.6	0.2	0.6	0.2	−0.3	6.0	0.1	5.6	4.3	9.8	4.1	9.8	−2.2	86.2	2.3	82.6	48.2	118.5	44.9	101.1
Hourly O_3	AIRBASE	649412	67.7	81.0	77.9	69.3	77.0	0.6	0.7	0.6	0.6	13.3	10.1	1.6	9.2	35.0	32.0	30.7	33.1	19.7	15.0	2.3	13.6	40.6	35.3	35.1	37.0
Hourly O_3	BDQA	97266	71.0	79.0	78.2	66.9	75.7	0.7	0.7	0.7	0.7	8.0	7.2	−4.1	4.7	31.5	29.8	29.1	29.7	11.2	10.1	−5.7	6.6	34.4	31.4	31.6	31.9
Max 1-h O_3	AIRBASE	41131	78.6	80.8	78.3	70.4	78.4	0.6	0.7	0.8	0.7	2.2	−0.3	−8.2	−0.2	28.2	28.9	27.1	31.3	2.7	−0.3	−10.5	−0.3	27.9	26.5	30.6	30.6
Max 1-h O_3	EMEP	4135	106.7	104.9	112.3	93.7	111.5	0.6	0.7	0.8	0.7	−1.8	5.6	−13.0	4.7	28.8	27.9	31.4	30.5	−1.5	5.2	−12.1	4.4	20.1	19.6	21.9	21.6
Max 8-h O_3	AIRBASE	27341	109	102.5	113.8	90.6	108.0	0.6	0.7	0.8	0.8	−8.4	2.9	−17.0	−2.9	26.3	25.4	28.7	28.4	−7.5	2.6	−18.3	−2.6	19.7	18.6	21.0	21.0
Max 8-h O_3	EMEP	1761	95.7	100.7	106.4	88.7	102.5	0.6	0.7	0.8	0.7	5.0	8.9	−7.0	6.8	24.3	25.8	23.3	25.5	5.4	9.3	−7.2	7.1	21.3	20.1	18.7	22.6
Hourly $PM_{2.5}$	BDQA	1726	99.8	98.2	105.9	86.3	99.5	0.7	0.7	0.8	0.6	−1.3	6.1	−1.6	6.1	22.9	23.6	23.6	27.8	−1.6	6.1	−1.7	6.1	18.8	19.1	18.8	19.7
Daily $PM_{2.5}$	AIRBASE	1902	12.9	11.3	21.6	12.1	21.7	0.5	0.5	0.4	0.4	1.1	8.6	−0.8	8.8	18.3	18.3	9.0	19.8	1.1	66.8	−6.4	67.9	41.1	86.8	50.0	91.8
Daily $PM_{2.5}$	EMEP	79	12.9	11.3	21.8	12.2	21.9	0.5	0.7	0.7	0.7	−1.6	9.0	−0.7	9.0	13.5	14.5	5.0	14.5	−12.5	69.0	−6.1	69.4	28.6	72.6	29.8	75.7
Hourly PM_{10}	AIRBASE	250	12.2	8.5	17.0	9.8	16.1	0.6	0.5	0.5	0.6	−3.7	4.8	−2.4	3.9	9.4	9.4	6.8	9.4	−30.6	39.4	−20.0	32.1	43.2	60.0	55.6	55.6
Hourly PM_{10}	BDQA	181957	23.9	11.9	21.5	13.1	21.6	0.3	0.2	0.3	0.2	−12.0	−2.3	−10.7	−2.3	19.9	18.3	19.6	19.5	−50.2	−9.8	−45.1	−9.5	58.3	53.2	53.2	55.8
Daily PM_{10}	AIRBASE	22667	19.4	12.3	23.5	13.3	23.9	0.4	0.3	0.4	0.3	−7.1	4.0	−5.9	3.2	14.5	18.1	14.5	16.6	−36.5	20.8	−31.5	13.0	64.2	72.6	60.0	60.0
Daily PM_{10}	BDQA	7847	23.9	11.9	21.6	13.1	21.9	0.2	0.5	0.4	0.3	−12.1	−2.3	−10.8	−2.2	12.5	11.2	15.1	12.2	−50.4	−9.8	−45.3	−9.4	52.5	60.0	48.7	60.0
Daily PM_{10}	AIRBASE	997	19.0	12.2	23.2	13.1	21.7	0.5	0.5	0.6	0.5	−6.9	4.6	−5.0	3.2	9.9	12.5	9.9	10.8	−37.3	24.9	−31.0	17.2	43.0	46.7	41.5	42.4
Daily PM_{10}	EMEP	488	15.5	10.5	19.5	11.5	17.8	0.5	0.4	0.5	0.4	−5.0	4.0	−4.0	2.2	8.8	10.6	8.2	9.1	−32.5	25.6	−25.9	14.4	46.7	47.4	41.6	42.2
SO_4^{2-}	EMEP	210	3.3	2.9	4.1	2.6	4.4	0.8	0.8	0.8	0.7	−0.4	0.8	−0.7	1.4	1.5	1.8	1.5	2.4	−21.4	24.5	−21.4	33.9	28.3	46.7	28.3	50.4
SO_4^{2-}	AIRBASE	643	2.9	2.4	3.9	2.2	4.0	0.6	0.6	0.6	0.5	−0.5	1.0	−0.6	1.7	1.7	2.2	1.8	2.5	−16.6	35.7	−21.8	39.8	55.9	40.0	38.1	62.1
NO_3^-	EMEP	210	2.6	4.2	10.3	5.6	10.8	0.5	0.6	0.5	0.5	1.4	7.0	2.3	1.0	2.5	8.7	3.7	10.1	42.0	212.3	71.3	226.7	57.4	215.6	70.7	230.1
NH_4^+	EMEP	109	2.6	7.4	10.3	4.5	10.8	0.5	0.5	0.5	0.5	4.8	5.5	1.9	5.5	7.1	9.1	3.9	8.2	63.0	184.6	71.3	212.3	201.6	104.9	71.3	216.3
NH_4^+	AIRBASE	106	2.0	2.3	3.5	2.4	3.8	0.4	0.7	0.7	0.6	0.3	1.5	0.4	1.8	1.1	2.2	1.3	3.2	13.8	73.9	20.5	89.1	34.3	81.1	20.5	102.9
Daily PM_{10} Cl^-	AIRBASE	162	2.0	1.9	2.2	2.1	3.1	0.4	0.4	0.4	0.6	−0.1	0.7	0.1	1.0	2.4	2.0	1.1	3.2	−8.1	33.0	3.7	89.1	44.5	74.3	3.7	85.0
Column CO	MOPPIT	15604	1.5	2.2	3.7	1.6	2.2	0.7	0.7	0.7	0.7	−1.5	3.0	1.6	2.8	4.5	4.5	2.4	2.7	235.7	452.0	147.5	235.0	251.5	461.3	147.5	251.0
Column NO_2	GOME	15432	1.5	1.5	2.2	1.5	2.2	0.8	0.3	0.8	0.7	3.0	0.6	1.6	0.7	7.1	8.7	3.7	2.4	−7.1	38.7	0.6	45.6	15.6	38.7	17.2	45.6
TOR	TOMS	9462	4.3	3.2	7.0	3.2	5.9	0.8	0.8	0.8	0.7	−1.9	2.0	1.2	1.6	2.9	3.6	2.3	3.6	−3.7	38.6	−26.5	36.9	38.1	47.9	33.1	53.1
AOD	MODIS	15604	0.2	56.6	28.1	54.7	28.5	0.8	0.7	0.6	0.3	−1.9	1.6	0.2	−14.4	15.1	14.6	12.2	14.6	35.7	−32.6	35.7	−33.7	35.7	32.6	33.7	75.8

[1] WP – WRF/Polyphemus; WC-S – WRF/Chem-MADRID simulations with the offline BVOC emissions of Simpson et al. (1999);
[2] the data pairs are based on the evaluation of predictions at a horizontal grid resolution of 0.125° over D02. Those based on the evaluation of predictions at a horizontal grid resolution of 0.5° over D02 are much smaller and not shown here;
[3] unit of concentration is µg m⁻³ for all surface chemical concentrations, 1×10^{18} molec cm⁻² for column CO, 1×10^{15} molec cm⁻² for column NO_2, and Dobson unit for TOR;
[4] WP – WRF/Polyphemus, WS – WRF/Chem-MADRID with BVOCs based on Simpson et al., 1999;
[5] the statistics from WRF/Chem-MADRID is in bold and the better one is in green, MB – mean bias, corr – correlation coefficient, RMSE – root mean square error, NMB – normalized mean bias, NME – normalized mean error.
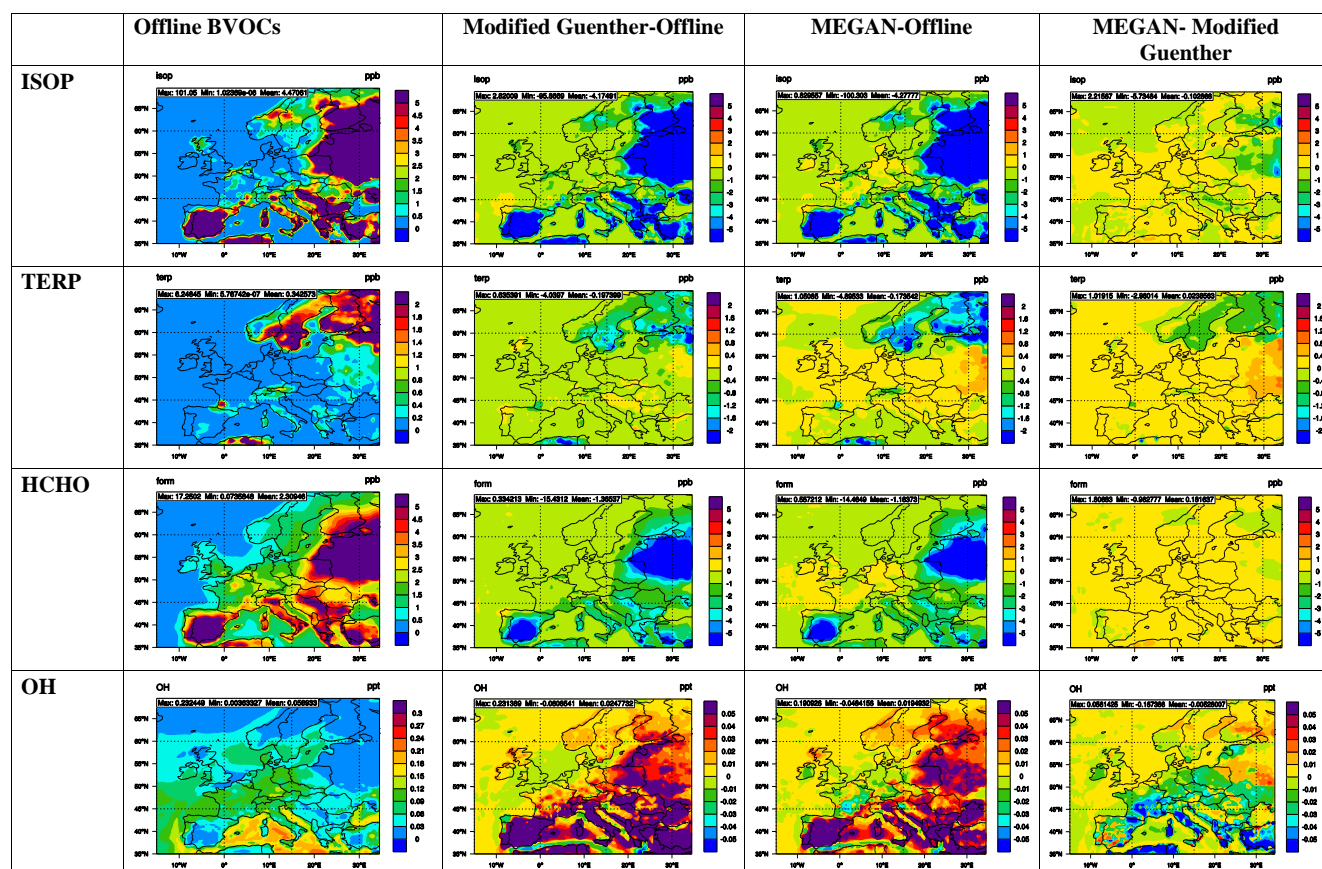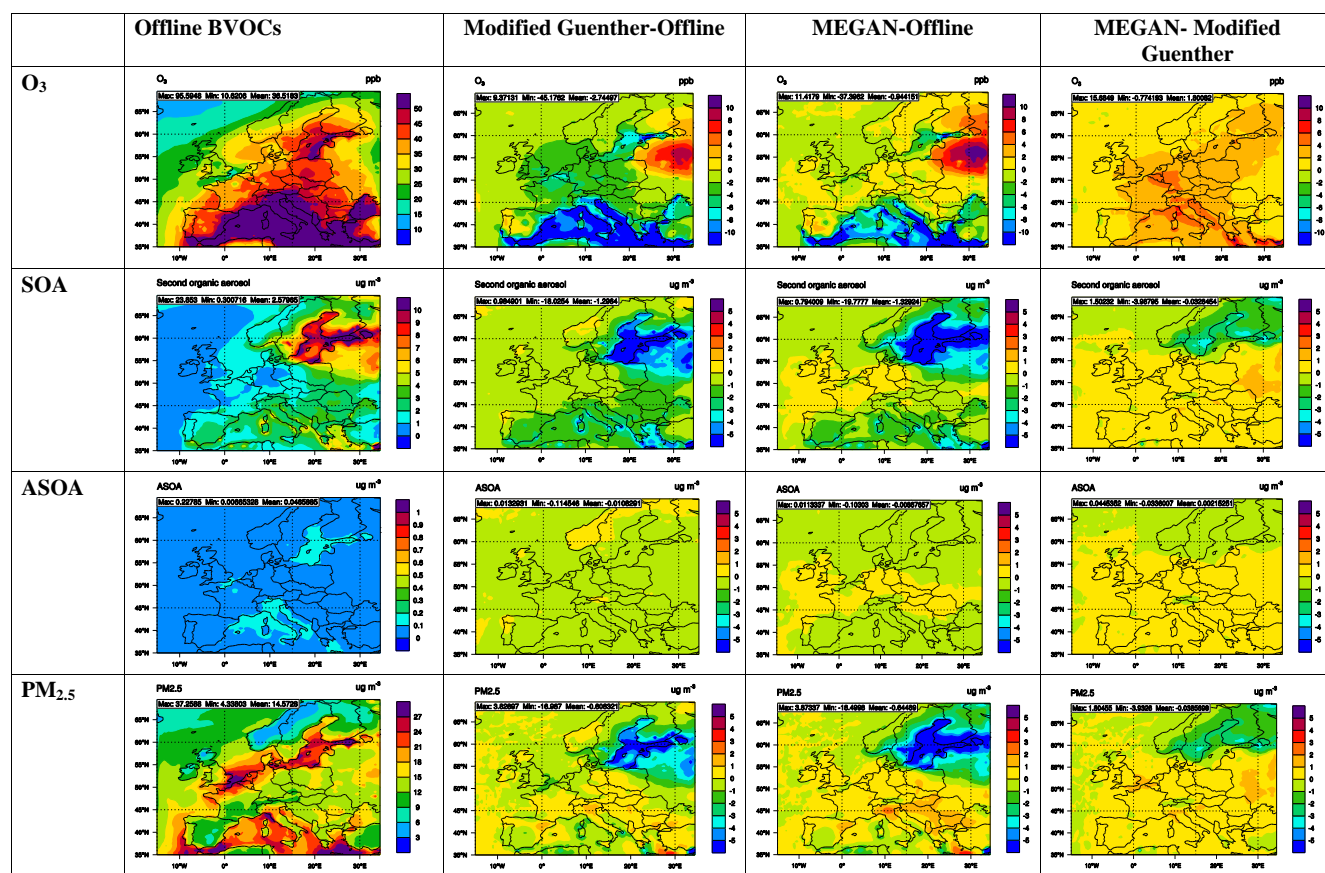
Fig. 10. Simulated concentrations of ISOP, TERP, HCHO, and OH by WRF/Chem-MADRID using offline BVOC emissions of Simpson et al. (1999) (column 1) and the absolute differences in their concentrations between simulations with modified Guenther online module and offline emissions (column 2), between simulations with MEGAN 2 online module and offline emissions (column 3), and between simulations with MEGAN 2 and modified Guenther online modules (column 4) in July 2001 over D01.

values than at 0.5°, leading to greater overpredictions on some days at these sites. For 24 h PM_{10} concentrations, WRF/Polyphemus at 0.125° gives slightly higher values at all sites except for Ispra, where the predictions at 0.125° are much higher, leading to a slightly better agreement with observations. WRF/Chem-MADRID at 0.125° may give either higher or lower values than at 0.5°, leading to better agreement at Deuselbach, Langenbrugge, Celje, Payerne, Niembro, and Ispra but worse at Tremblay-en-France, Ternay, Chaumont, and Cabo de Creus.

Table 2 shows the corresponding domainwide performance statistics for those species and additional species, such as NH_3, HNO_3, and PM_{10} composition SO_4^{2-}, NO_3^-, NH_4^+, Na^+, and Cl^- at 0.125° over D02 and compares them with those from the simulation at 0.5° but over the same D02 domain to examine the sensitivity of the model predictions to horizontal grid resolutions. For performance statistics at 0.125° over D02, compared with WRF/Chem-MADRID, WRF/Polyphemus performs better for NH_3, HNO_3, daily SO_2, and NO_2 at the EMEP sites, hourly O_3, maximum 1 h O_3 at the EMEP sites, maximum 8 h O_3 at the Air-

Base and BDQA sites, hourly and daily $PM_{2.5}$, PM_{10} composition at all sites, and column CO and NO_2. It performs worse for hourly SO_2 and NO_2 at the AirBase and BDQA sites, hourly O_3, maximum 1 h O_3 at the BDQA and EMEP sites, maximum 8 h O_3 at the EMEP sites, PM_{10}, TOR, and AOD. For both models, the use of a finer grid resolution leads an overall better performance for most variables. For WRF/Polyphemus, the use of a finer grid resolution improves the model performance in terms of NMBs for all variables evaluated except for daily HNO_3, hourly O_3 against EMEP, maximum 1 h and 8 h O_3 at all sites, daily SO_4^{2-}, daily NO_3^-, daily NH_4^+ against AirBase, column NO_2, and AOD. The relatively large improvement (reducing NMBs by 5 % or more from their values at 0.5°) occurs for hourly and daily NH_3, hourly SO_2 against BDQA, hourly NO_2 and hourly O_3 against AirBase and BDQA, hourly and daily $PM_{2.5}$ and PM_{10}, daily Cl^-, column CO, and TOR. For WRF/Chem-MADRID, the use of a finer grid resolution improves the model performance in terms of NMBs for all variables evaluated except for daily HNO_3, hourly SO_2 against AirBase,

Fig. 11. Simulated concentrations of O3, SOA, ASOA, and PM$_{2.5}$ species by WRF/Chem-MADRID using offline BVOC emissions of Simpson et al. (1999) (column 1) and the absolute differences in their concentrations between simulations with modified Guenther online module and offline emissions (column 2), between simulations with MEGAN 2 online module and offline emissions (column 3), and between simulations with MEGAN 2 and modified Guenther online modules (column 4) in July 2001 over D01.

hourly NO$_2$ against BDQA, maximum 8 h O$_3$ against EMEP, hourly and daily PM$_{2.5}$ against AirBase, daily SO$_4^{2-}$, daily NO$_3^-$, daily NH$_4^+$, and column CO, NO$_2$, and TOR. The relatively large improvement occurs for hourly SO$_2$ against BDQA, daily SO$_2$ and NO$_2$ against EMEP, maximum 8 h O$_3$ against BDQA, daily PM$_{2.5}$ against EMEP, hourly PM$_{10}$ against BDQA, daily PM$_{10}$ against BDQA and EMEP, and AOD. As shown, the use of a finer grid resolution does not always improve model performance, nor does not give an expected significant improvement for all species. Similar results were obtained by Bailey et al. (2007), who found better performance for O$_3$ at a finer spatial resolution (8 km), but better performance for PM at a coarser resolution (32 km) over the eastern US. Possible reasons can be attributed to inaccuracies or uncertainties in the required inputs (e.g., meteorology, emissions, and land use) at a finer grid resolution due to the limitation of current meteorological models in capturing fine-scale atmospheric processes and the lack of information at a finer grid scale. The grid-averaging of emissions and land use data can influence model predictions. An aver-

aging over a coarser grid resolution may sometimes smooth the spatial distribution of the variables concerned (e.g., emissions), leading to a better agreement with observations, although the representation may not be more accurate.

4.2   Sensitivity to biogenic emissions

Different BVOC modules produce significantly different BVOC emissions in terms of total emissions and their spatial distributions. For example, the domain-average emission fluxes of isoprene (ISOP) and formaldehyde (HCHO) are 8.1 and 0.05, 1.9 and 0.06, and 2.5 and 0.07 mol km^{-2} h^{-1} for the offline BVOC emissions based on Simpson et al. (1999), online BVOC emissions based on modified Guenther of Guenther et al. (1993, 1999) and MEGAN of Guenther et al. (2006) (referred to as WC-S, WC-G, and WC-M, respectively), respectively. Different BVOC emissions result in different chemical predictions from the three simulations, in particular, concentrations of BVOCs, oxidants, radicals, and secondary species that are strongly affected by oxidants and radicals. Figures 10 and 11 show simulated concentrations

Table 3. Characteristics of sites selected for temporal analysis.

| Country	Site name	Site ID (network)	Site Type	Latitude	Longitude	Elevation (m)	Characteristics
Austria	Illmitz	AT02 (EMEP)	Rural Background	47.78° N	16.77° E	117	Located on the eastern shore of Lake Neusiedl in eastern Austria. It has oceanic climate, featuring warm but not hot summers and cool but not cold winters.
Denmark	Keldsnor/ 9055	DK0048A (AirBase)	Rural	54.75° N	10.74° E	10	A coastal site located in southeastern Denmark. The climate is in the temperate climate zone with cold winters and warm summers.
Finland	Mansikkala	FI00424 (AirBase)	Suburban Background	61.19° N	28.77° E	100	Located in the town of Imatra in southern Finland. It has subarctic climate with cool summer, severe winter, and no dry season.
	Kallio_2	FI0124A (AirBase)	Urban Background	60.19° N	24.95° E	21	Located in Helsinki. This region has a hemiboreal humid continental climate. Owing to the mitigating influence of the Baltic Sea and Gulf Stream, temperatures in winter are much higher than the far northern location, with the average around -5 °C. The summer average maximum temperature is 19–21 °C. However, because of the latitude, it has 19 h daytime in summer and < 6 h daytime in winters.
France	Melun	FR04069 (AirBase, BDQA)	Urban	48.54° N	2.66° E	56	See Table 5, Part 1.
	Nord-Est Alsace	FR16017 (AirBase, BDQA)	Rural	48.92° N	8.16° E	114	Located in northeastern Alsace, a city on France's eastern border and on the west bank of the upper Rhine adjacent to Germany and Switzerland. Alsace has a semi-continental climate with cold and dry winters and hot summers, and little precipitation
	Sommet Puy de Dôme	FR07015 (AirBase, BDQA)	Rural	45.77° N	2.96° E	1460	Located on the top of the Puy-de-Dôme in south-central France. Annual average summer high temperature is 25 °C and winter low temperature is -1 °C, with annual precipitation 592 m and snow coverage on top of the mountains through May.
	Ternay	FR20037 (AirBase, BDQA)	Suburban	45.60° N	4.80° E	235	Located ~ 18 km south of Lyon. The weather in this region is on the borderline of oceanic and humid subtropical climate, with very warm summers (21.3 °C on average) and colder winters (3.2 °C on average) than much of the south of France due to its more inland position. Annual average total precipitation is 840 mm, with the winter months the driest.
	Tremblay-en-France	FR04319 (AirBase, BDQA)	Suburban	48.95° N	2.57° E	65	In the northeastern suburbs of Paris (~ 19.5 km from Paris).
Germany	Deuselbach	DE04 (EMEP)	Rural	49.76° N	7.05° E	480	Located ~ 150 km southwest of Cologne in southwestern Germany. It has an oceanic climate, with annual mean summer and winter temperatures of 16.3 °C and -0.6 °C, respectively.
	Düsseldorf-Lörick	DENW071 (AirBase)	Suburban Background	51.25° N	6.73° E	32	See Table 5, Part 1.
	Langenbrugge	DE02 (EMEP)	Rural	52.80° N	10.76° E	74	Located on a hill above the river Jagst, 18 km northeast of Schwäbisch Hall in southern Germany. This area has an oceanic climate, with warm summer (average high temperature of 24 °C) and cold winter (average low temperature of -3 °C).
Italy	Ispra	IT04 (EMEP)	Suburban	45.8° N	8.63° E	209	Located on the eastern shore of Lake Maggiore, ~ 60 km northwest of Milan in the northwest Italy. It has an oceanic climate and is affected by lake breezes.
Norway	Birkenes	NO01 (EMEP)	Rural	58.38° N	8.25° E	190	A coastal site ~ 30 km from Kristiansand in southern Norway. It has an oceanic climate, with summers average daytime temperatures of 15.7–20.1 °C and snowy winters with average temperatures of -0.9 to 1.3 °C. Annual precipitation is very high (1380 mm).
Portugal	Beato	PT03070 (AirBase)	Urban Background	38.73° N	9.11° W	56	A coastal site in Lisbon. Lisbon has a subtropical Mediterranean climate, with mild, rainy winters and warm to hot and dry summers. Among all the metropolises in Europe, it has the warmest winters, with average temperatures of 8–15 °C. The typical summer high temperatures are 26 to 34 °C.
	Custóias	PT01021 (AirBase)	Suburban Background	41.20° N	8.65° E	100	Located in the Greater Porto area, where the Mediterranean climate prevails, with warm, dry summers and mild, rainy winters. Summers average temperatures between 15 and 25 °C. Winter temperatures typically range between 5 and 15 °C. The annual precipitation is 1253 mm.
	Ermesinde	PT01023 (AirBase)	Suburban Background	41.21° N	8.55° E	140	Located ~ 9 km northeast of Porto in Portugal.
Slovakia	Topolniky	SK07 (EMEP)	Urban	47.96° N	17.86° E	113	Located in the plain terrain of the Danubian lowlands in northwestern Slovakia. The area has a warm temperate climate.
Slovenia	Celje	SI0001A (AirBase)	Urban	46.24° N	15.27° E	240	The third largest town in the east Slovenia. It has a warm temperate climate with warm summers and some rainfall in all months. The summer high temperatures can reach 36.8 °C, and the winter low temperature is -4.7 °C. Annual precipitation is ~ 142 mm.

Table 3. Continued.

Country	Site name	Site ID (network)	Site Type	Latitude	Longitude	Elevation (m)	Characteristics
Spain	Avenida Gasteiz	ES1502A (AirBase)	Urban	42.85° N	2.68° W	517	Located in northern Spain. It has a mild humid temperate climate with warm summers and no dry season. The annual summer high temperature is 26.7 °C, and the winter low temperature is 1.1 °C.
	Cabo de Creus	ES10 (EMEP)	Rural Background	42.32° N	3.32° W	23	Located in the Cap de Creus peninsula. This region features a Mediterranean climate. Summers are dry and hot with sea breezes, and the maximum temperature is around 26–31 °C. Winter is cool or slightly cold with occasional snow.
	Els Torms	ES14 (EMEP)	Rural Background	41.40° N	0.72° E	470	Located in the province of Catalonia in northeastern Spain. This region features a Mediterranean climate.
	Niembro	ES08 (EMEP)	Rural Background	43.44° N	4.85° W	134	A beach site in the province of Asturias in northern Spain. It has a maritime climate. Summers are generally humid and warm with some rain. Winters are cold with some very cold snaps and snow.
Sweden	Rörvik	SE02 (EMEP)	Rural	57.42° N	11.93° E	10	A coastal site located ∼ 40 km south of Gothenburg and surrounded by an open Scots pine forest. It has an oceanic climate.
	Femman	SE0004A (AirBase)	Urban	57.71° N	11.97° E	30	A roof site in the Gothenburg. Due to the Gulf Stream, this area has oceanic climate and frequent rain. Summers are warm with average high temperatures of 19 to 20 °C. Winters are cold and windy with temperatures of around −5 to 3 °C. The daytime is 17 h, and the nighttime is ∼ 7 h due to a high latitude.
	Södermalm	SE0022A (AirBase)	Urban	59.32° N	18.06° E	20	See Table 5, Part 1.
	Sundsvall	SE0028A (AirBase)	Urban Background	62.39° N	17.31° E	10	On the east coast, and middle portion of Sweden. It has a climate on the border between subarctic and cold continental, with summer high temperatures of 21 °C and winter low temperature of −15 °C.
Switzerland	Chaumont	CH04 (EMEP)	Rural	47.05° N	6.98° E	1130	In the mountain Chaumont in the city of Neuchâtel. Chaumont has humid continental climate with warm summer (average high temperature is 24.0 °C) and humid with severe winter (average low temperature is −1.4 °C).
	Payerne	CH02 (EMEP)	Suburban	46.82° N	6.95° E	510	In western Switzerland. It has an oceanic climate, with the summer average high temperature of 24.1 °C and the winter average low temperature of −3.3 °C. Payerne has an average of 116.4 days of rain or snow per year and on average receives 845 mm of precipitation, with August the wettest and February the driest.
UK	Harwell	GB0036R (AirBase)	Rural	51.57° N	1.32° W	137	Located ∼ 81 km northwest of London in southern UK. It has a maritime temperate climate.
	Rochester Stoke	GB0617A (AirBase)	Rural	51.46° N	0.63° E	14	Located in the city of Rochester in the southeastern corner of England, UK. It has a maritime temperate climate, one of the warmest parts of UK, with summer average high temperature of 21.9 °C and winter average lower temperature of 1.7 °C.
	London Bloomsbury	GB0566A (AirBase)	Urban Background	51.52° N	0.12° W	20	See Table 5, Part 1.

of ISOP, terpenes (TERP), HCHO, OH, O_3, SOA, anthropogenic SOA (ASOA), and $PM_{2.5}$ from the simulation WC-S and the absolute differences in these concentrations between WC-G and WC-S, and between WC-M and WC-S over D01 in July 2001. WC-S gives the highest BVOC emissions domainwide, leading to the highest domainwide concentrations of BVOCs, HCHO, higher aldehydes, and HO_2, which in turn lead to the highest domainwide concentrations of O_3, SOA, ASOA, and $PM_{2.5}$. Compared to WC-G, WC-M gives higher TERP and ISOP emissions over most areas, leading to higher HCHO concentrations for almost the whole domain. Although WC-M gives lower terpene concentrations in Sweden, Finland, and a portion of Russia, it produces higher terpene concentrations over the rest of domain, leading to higher domain-average concentrations of terpene than WC-G. High HO_2 concentrations resulting from higher HCHO and TERP convert more NO to NO_2, leading to higher O_3 by WC-M than by WC-G. On the other hand, higher BVOC emissions from WC-M consume more OH, lead-

ing to slightly lower OH concentrations, thus slightly lower domain-average concentrations of ISOP, SOA, and $PM_{2.5}$ (despite higher concentrations of SOA and $PM_{2.5}$ in some areas such as Romania, Ukraine, and Belarus). The SOA formation is dominated by biogenic SOA (BSOA) in the whole domain, with very small contributions from ASOA in a few areas. Different BVOC emissions will thus affect mostly biogenic SOA, although they also affect the formation of ASOA through affecting oxidants and radicals. For example, compared to the simulation with offline BVOCs, the simulation using MEGAN BVOC module gives lower SOA and BSOA concentrations, by 1.32 μg m⁻³ domainwide mean (−30 %) and as low as −9.7 μg m⁻³ (by −92.5 %), and it gives lower ASOA concentrations, by 0.009 μg m⁻³ domainwide mean and as low as 0.06 μg m⁻³. Spatially, ISOP and TERP correlate well with SOA, which is an important contributor for $PM_{2.5}$ over regions with high BVOC emissions. Table 1 compares performance statistics of WRF/Chem-MADRID using three different BVOC modules over D01. The performance
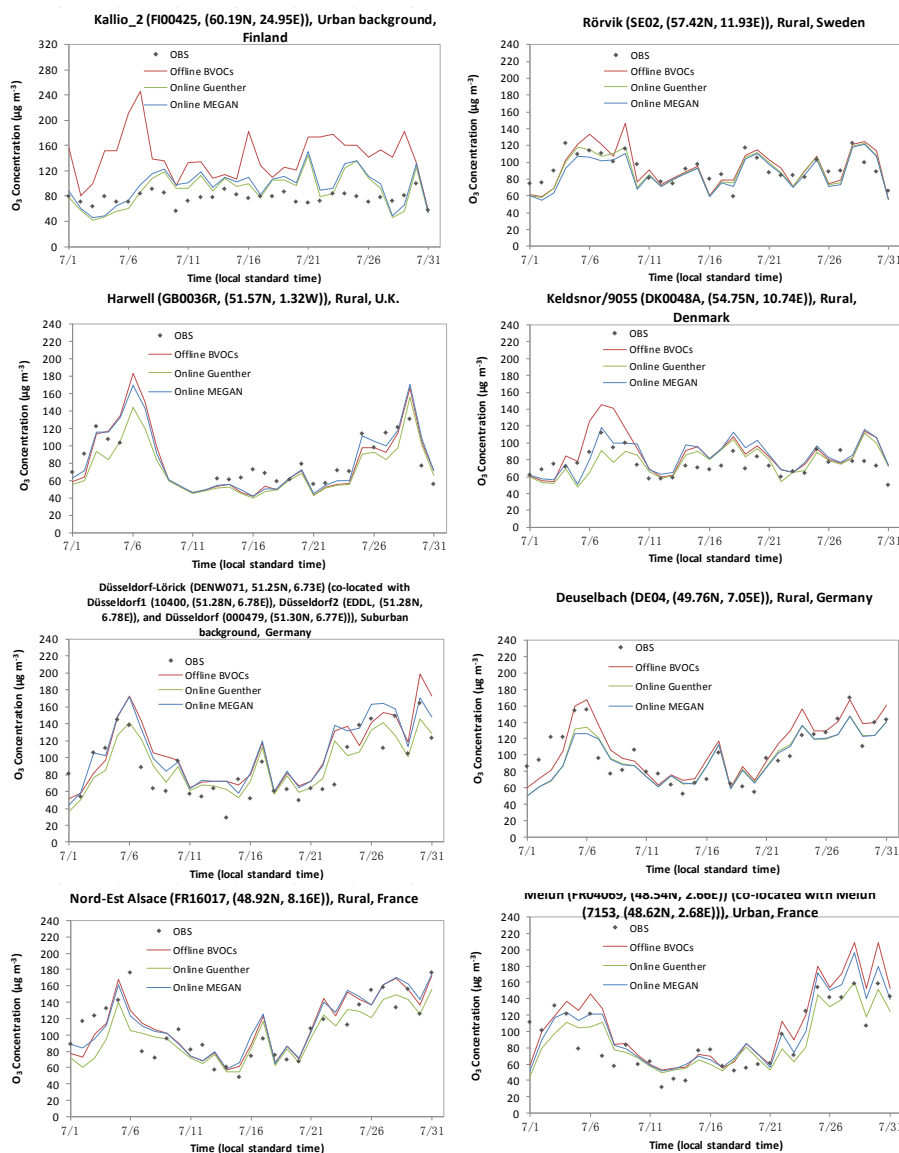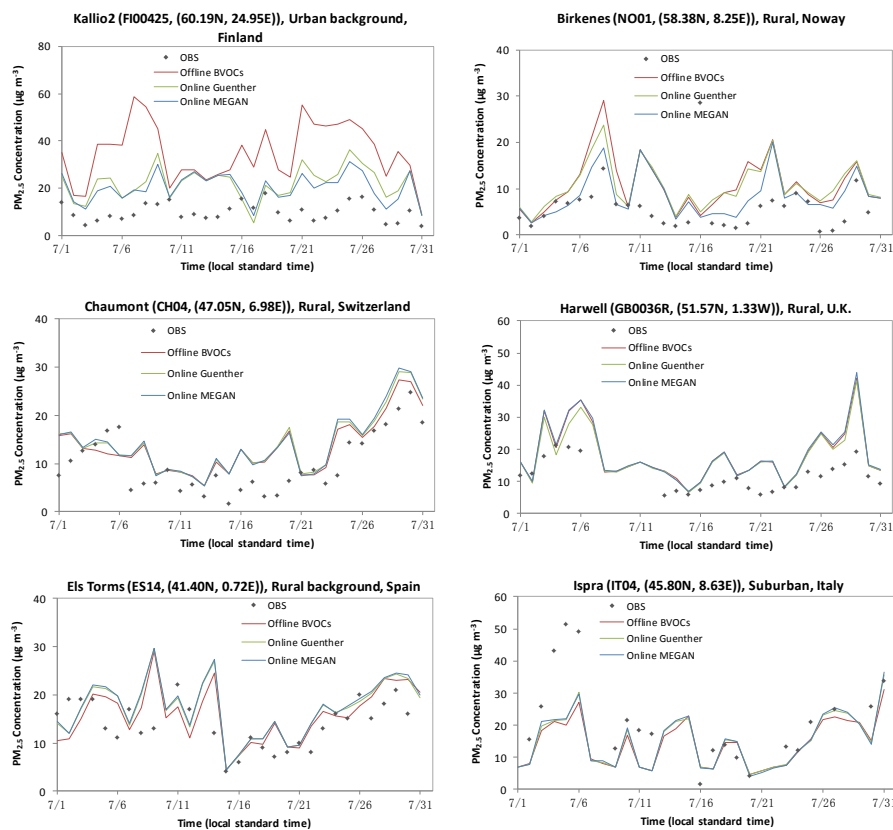
Fig. 12. Simulated and observed concentrations of max 8 h O_3 over D01 from WRF/Chem-MADRID using offline BVOC emissions of Simpson et al. (1999) and online BVOC emission modules based on modified Guenther (Guenther et al., 1995) and MEGAN (Guenther et al., 2006) in July 2001 at selected sites over D01.

statistics is overall similar. WC-S gives slightly better agreement in terms of NMBs for NH_3, HNO_3, hourly NO_2, maximum 1 h O_3 at the EMEP sites, daily PM_{10} at the EMEP sites, daily SO_4^{2-}, daily NO_3^- at the EMEP sites, NO_3^-, NH_4^+, Na^+, and Cl^- at the AirBase sites, and column NO_2. WC-G gives slightly better agreement in terms of NMBs for hourly SO_2, daily NO_2, maximum 8 h O_3 at the AirBase and EMEP sites, hourly PM_{10} at the BDQA sites, daily NO_3^- at the Air-Base sites, column CO, and AOD, and WC-M gives slightly better agreement in terms of NMBs for daily SO_2, maximum 1 h O_3 at the AirBase and BDQA sites, maximum 8 h O_3 at the BDQA sites, hourly $PM_{2.5}$ and PM_{10} at the AirBase

sites, daily Cl^- at the EMEP sites, and TOR. WC-G gives much better hourly O_3 performance than the other two simulations. WC-S and WC-G give the same agreement for daily $PM_{2.5}$ at the EMEP sites. Among the species evaluated, those that are relatively more sensitive to different BVOC modules include HNO_3, hourly and maximum 8 h O_3, hourly $PM_{2.5}$, SO_4^{2-}, NO_3^-, NH_4^+, and AOD.

Figures 12–13 show observed and simulated temporal variations of maximum 8 h O_3 and 24 h $PM_{2.5}$ concentrations at specific sites from the three simulations using WRF/Chem-MADRID with different BVOC emissions. O_3 formation is very sensitive to BVOC emissions at Kallio

Fig. 13. Simulated and observed concentrations of 24 h average PM$_{2.5}$ over D01 from WRF/Chem-MADRID using offline BVOC emissions of Simpson et al. (1999) and online BVOC emission modules based on modified Guenther (Guenther et al., 1995) and MEGAN (Guenther et al., 2006) in July 2001 at selected sites over D01.

in Finland, moderately sensitive at Rörvik, Sweden, Keld-snor/9055 in Denmark, Deuselbach in Germany, and Melun in France, and slightly sensitive at the remaining sites. WC-S tends to overpredict maximum 8 h O$_3$ at all sites except for Deuselbach, where it gives the best agreement with observations among the three simulations. WC-G gives the best agreement at Rörvik, Harwell, Düsseldorf-Lörick, Kallio_2, and Melun. WC-M gives the best agreement at Keldsnor/9055 and Nord-Est Alsace. The 24 h PM$_{2.5}$ concentrations are also very or moderately sensitive to BVOC emissions at some sites (e.g., Kallio_2 and Birkenes), although they are slightly sensitive at the remaining sites. While WC-S significantly overpredicts PM$_{2.5}$ concentrations at Kallio_2 and Birkenes, it gives an overall best agreement at Chaumont and Els Torms. WC-M gives the best agreement at Kallio_2 and Birkenes. The simulations with the three different BVOCs give similar results at Harwell and Ispra.

5   Impact of aerosols on gaseous pollutant predictions

As shown in Fig. 14, the emissions of primary SO$_4^{2-}$ and NO$_3^-$, and gaseous precursors for secondary aerosol lead to

high concentrations of NH$_4^+$, SO$_4^{2-}$ and NO$_3^-$ in the whole domain. Their formation would affect the levels of oxidants and radicals available for oxidation of gaseous species, as they compete for the same sets of oxidants and radicals. As shown in Fig. 5 in Part 1, those secondary aerosols together with primary aerosols can affect many meteorological variables in different ways. The changes in meteorological variables due to aerosol–meteorology interactions in turn affect the chemical predictions of gaseous concentrations in the next time step. Fig. 14 also shows the impact of aerosols on gaseous predictions through secondary aerosol formation processes and aerosol–meteorology interactions. For example, in the presence of PM, the CO concentrations are higher due to reduced WS10, reduced PBL height, and a lower amount of OH radicals available for its oxidation as a result of competitive consumption of these radicals by PM precursors to form secondary aerosols. As a result of a similar competition, the concentrations of O$_3$ are lower due to a lower amount of radicals (e.g., OH and HO$_2$) available to oxidize the precursors of O$_3$. The concentrations of NH$_3$ and HNO$_3$ are lower due to a higher amount of NH$_4$NO$_3$ formation that compensates their potential increase caused by a reduced PBL height. The concentrations of SO$_2$ are
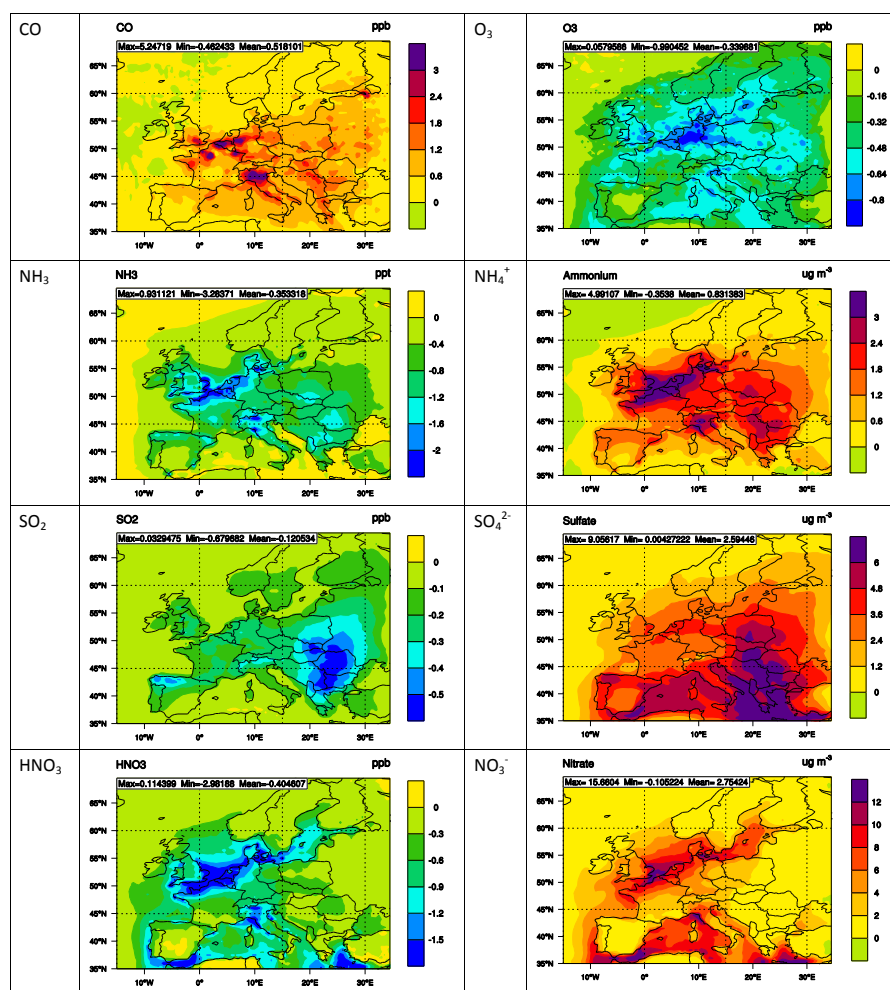
Fig. 14. Simulated changes in chemical composition in the presence of aerosol by WRF/Chem-MADRID in July 2001 over D01.

lower due to a higher conversion rate to form SO_4^{2-} that resulted from increased temperature. These results caused by secondary aerosol formation and meteorology–chemistry interactions are consistent with the simulated aerosol effects using GU-WRF/Chem over the global domain and nested domains over North America and East Asia reported by Zhang et al. (2012b).

6 Conclusions

In this Part 2, the offline-coupled model (WRF/Polyphemus) and the online-coupled model (WRF/Chem-MADRID) are applied to simulate air quality in July 2001 at horizontal grid resolutions of 0.5° and 0.125° over Western Europe. To minimize differences caused by model inputs, both models use the same version of WRF to generate meteorological predictions and the same anthropogenic emissions. They also use the same model mechanisms (e.g., CB05 for gas-phase mechanism, Fast-J for photolysis scheme, and

Carnegie Mellon University (CMU) mechanism for aqueous-phase chemistry). Differences remain in their vertical structures (e.g., heights of the first model layer, thickness of each layer, and the total number of model layers), chemical initial and boundary conditions, emissions of dust and sea salt, heterogeneous chemistry, dry and wet deposition, aerosol treatments, and aerosol–cloud interactions. A comprehensive model evaluation is performed to evaluate the model's performance using three surface monitoring stations including EMEP, AirBase, and BDQA and several satellite databases including MOPPIT, GOME, TOMS, and MODIS.

For domainwide statistical performance at 0.5°, compared with WRF/Polyphemus, WRF/Chem-MADRID gives higher domainwide mean values for all surface concentrations and column variables except for hourly O_3 and TOR (which differs substantially due to the use of different upper layer boundary conditions). Compared with observations, WRF/Polyphemus gives better statistical performance for daily HNO_3, SO_2, and NO_2 at the EMEP sites, maximum 1 h O_3 at the AirBase sites, maximum 8 h O_3 at all sites, $PM_{2.5}$

at the AirBase sites, PM_{10} composition, column abundance of CO, NO_2, and TOR, and AOD, whereas WRF/Chem-MADRID outperforms for NH_3, hourly SO_2, NO_2, and O_3 at the AirBase and BDQA sites, maximum 1 h O_3 at the BDQA and EMEP sites, and PM_{10} at all sites. For spatial distribution at 0.5°, compared with WRF/Polyphemus, WRF/Chem-MADRID gives higher values over most of the domain, in particular, over polluted regions in Central and southern Europe for all surface concentrations and column variables except for TOR. The model performance in terms of temporal variation varies from site to site, depending on the latitude bands, topography, meteorological and climate conditions, and source of pollutants. For temporal distributions of SO_2, WRF/Chem-MADRID reproduces well the observed high concentrations at urban and suburban sites except for extremely high episodes at a few sites, and WRF/Polyphemus performs well at rural and some background sites where pollutant levels are relatively low. For temporal distributions of NO_2, WRF/Chem-MADRID reproduces well the observed concentrations at most sites, whereas WRF/Polyphemus underpredicts them at most sites. For temporal distributions of O_3, both models generally capture well the daytime maximum 8 h O_3 concentrations at all sites except for urban/suburban background sites where both models overpredict the observations. They both generally simulate well the diurnal variations of O_3 with more accurate peak daytime and minimal nighttime values by WRF/Chem-MADRID, but neither model reproduces extremely low nighttime O_3 concentrations at several urban and suburban sites due to underpredictions of NO_x and thus insufficient titration of O_3 at night. For temporal distributions of $PM_{2.5}$, WRF/Polyphemus gives more accurate predictions in terms of magnitudes, and WRF/Chem-MADRID overpredicts at all sites. For temporal distributions of PM_{10}, WRF/Chem-MADRID reproduces reasonably well the observations at all sites but due mainly to the overpredictions of $PM_{2.5}$, whereas WRF/Polyphemus significantly underpredicts them. The predictions of column variables differ significantly between the two models. WRF/Polyphemus gives relatively good performance for column CO and NO_2 in terms of domainwide statistics, but fails to reproduce high observed column CO concentrations in most regions. WRF/Chem-MADRID significantly overpredicts column CO and NO_2 but captures better their high column mass concentrations. WRF/Polyphemus gives much higher TOR than WRF/Chem-MADRID, but neither model captures the observed magnitudes of TOR. Both models significantly overpredict AOD.

These differences in model predictions of gaseous pollutants and $PM_{2.5}$ are caused by differences in vertical structure that causes differences in vertical distributions of emissions, boundary conditions of some species (e.g., O_3 and CO), heterogeneous chemistry, dry and wet deposition treatments of gases (e.g., SO_2 and NO_2) and PM species (SO_4^{2-}, NO_3^-, NH_4^+, BC, and TOM), aerosol treatments such as inorganic

aerosol thermodynamics and SOA, as well as aerosol–cloud interactions used in both models. Additional differences in $PM_{2.5}$ and PM_{10} predictions are due to the fact that the two models use different boundary conditions for dust particles and sea-salt emission modules, and WRF/Chem-MADRID uses an online soil dust emission module that is not included in WRF/Polyphemus. The inclusion of soil dust emissions allows a better representation of PM_{10} concentrations. The differences between model predictions and observations are mostly caused by inaccurate representations of emissions of gaseous precursors such as SO_2, NO_2, and VOCs and primary PM such as EC and POC during the high pollution episodes in the EMEP emission inventories. Both models fail to reproduce nighttime O_3 levels, due mainly to underpredictions in NO_x emissions and thus insufficient titration of nighttime O_3 under the high-NO_x conditions and missing mechanisms of O_3 destruction such as the heterogeneous reactions of sea salt in the models under the low-NO_x conditions. Some of the differences between chemical predictions and observations can also be attributed to biases in the meteorological predictions such as 2 m temperature and 10 m wind speed.

Both models show some sensitivity to horizontal grid resolutions, in particular, at mountain/high altitude sites and sites with complex terrain. Compared with WRF/Polyphemus, WRF/Chem-MADRID shows a higher sensitivity to grid resolutions at all sites. For both models, the use of a finer grid resolution generally leads to an overall better statistical performance for most variables, with greater details in areas having high or low concentrations and an overall better agreement in temporal variations and magnitudes at most sites. The use of a finer grid resolution, however, does not always improve model performance due to the limitation of current meteorological models in capturing fine-scale atmospheric processes and the lack of information for a more accurate representation of emissions and land use data at a finer grid scale.

Different BVOC emission modules generate significantly different BVOC emissions in terms of magnitudes of total emissions and their spatial distributions, which in turn affect chemical predictions. WRF/Chem-MADRID sensitivity simulations show moderate to large differences in predicted concentrations of BVOCs, HCHO, OH, O_3, SOA, and $PM_{2.5}$ between the offline and online emissions but a similarity between the simulations with the two online BVOC emission modules. The use of online BVOC emissions gives better statistical performance for hourly and maximum 8 h O_3 and $PM_{2.5}$ and generally better agreement with their observed temporal variations at most sites.

Therefore, it appears that major sources of uncertainties in current state-of-the-science air quality models are the vertical structure of the models (i.e., heights of the first model layer, thickness of each layer, and the total number of model layers), inputs (i.e., vertical distributions of emissions, natural emissions of dust, sea salt, and BVOCs, and boundary

conditions) and removal (i.e., dry and wet deposition rates of gases and particles) of pollutants. These results suggest that, on the one hand, the transport and transformation processes of most pollutants are mostly well represented, but that, on the other hand, experimental data on emissions (in particular, the vertical distribution of emissions) and deposition are in dire need of refinement if one wants to improve model performance. In addition, boundary conditions generated using different models may introduce large differences, in particular, the column mass abundance of chemical species such as O_3 and CO.

As an online-coupled meteorology–chemistry model, WRF/Chem-MADRID can simulate various feedbacks between meteorology and chemical species. Such feedbacks can in turn affect chemical predictions of all species. These results are consistent in sign but smaller in terms of magnitudes as compared with the simulated aerosol effects found by previous studies over other regions of the world, such as East Asia and North America.

References

Anttila, P. and Salmi, T.: Characterizing temporal and spatial patterns of urban PM_{10} using six years of Finnish monitoring data, Boreal. Environ. Res., 11, 463–479, 2006.

Aphesis (Air Pollution and Health: A European Information System): Health impact assessment of air pollution In 26 European Cities, ENHIS-1 Project: WP5 Health impact assessment, Second-year Report, 2000–2001, http://www.apheis.org/index.html, 2006.

Arunachalam, S., Holland, A., Do, B., and Abraczinskas, M.: A quantitative assessment of the influence of grid resolution on predictions of future-year air quality in North Carolina, USA, Atmos. Environ., 40, 5010–5026, 2006.

Bailey, E. M., Gautney, L. L., Kelsoe, J. J., Jacobs, M. E., Condrey, J.W., Pun, B., Wu, S.-Y., Seigneur, C., Douglas, S., Haney, J., and Kumar, N.: A comparison of the performance of four air quality models for the Southern Oxidants Study episode in July 1999, J. Geophys. Res., 112, D05306, doi:10.1029/2005JD007021, 2007.

Barmpadimos, I., Keller, J., Oderbolz, D., Hueglin, C., and Prévôt, A. S. H.: One decade of parallel fine ($PM_{2.5}$) and coarse (PM_{10}–$PM_{2.5}$), particulate matter measurements in Europe: trends and variability, Atmos. Chem. Phys., 12, 3189–3203, doi:10.5194/acp-12-3189-2012, 2012.

Chin, M., Rood, R., Lin, S.-J., Muller, J., Thompson, A.: Atmospheric sulfur cycle in the global model GOCART: model description and global properties, J. Geophys. Res., 105, 24671–24687, 2000.

Cohan, D. S., Hu, Y., and Russell, A.G.: Dependence of ozone sensitivity analysis on grid resolution, Atmos. Environ., 40, 126–135, 2006.

de Meij, A., Krol, M., Dentener, F., Vignati, E., Cuvelier, C., and Thunis, P.: The sensitivity of aerosol in Europe to two different emission inventories and temporal distribution of emissions, Atmos. Chem. Phys., 6, 4287–4309, doi:10.5194/acp-6-4287-2006, 2006.

Fast, J. D., Gustafson Jr., W. I., Easter, R. C., Zaveri, R. A., Barnard, J. C., Chapman, E. G., Grell, G. A., and Peckham, S. E.: Evolution of ozone, particulates, and aerosol direct radiative forcing in the vicinity of Houston using a fully coupled meteorology-chemistry-aerosol model, J. Geophys. Res., 111, D21305, doi:10.1029/2005JD006721, 2006.

Forkel, R., Werhahn, J., Hansen, A. B., McKeen, S., Peckham, S., Grell, G., and Suppan, P.: Effect of aerosol-radiation feedback on regional air quality – A case study with WRF/Chem, Atmos. Environ., 53, 202–211, 2012.

Guenther, A., Zimmerman, P., Harley, P., Monson, R., and Fall, R.: Isoprene and monoterpene emission rate variability: model evaluation and sensitivity analysis, J. Geophys. Res, 98, 12609–12617, 1993.

Guenther, A., Baugh, B., Brasseur, G., Greenberg, J., Harley, P., Klinger, L., Serca, D., and Vierling, L.: Isoprene emission estimates and uncertainties for the Central African EXPRESSO study domain, J. Geophys. Res.-Atmos., 104, 30625–30639, 1999.

Guenther, A., Karl, T., Harley, P., Wiedinmyer, C., Palmer, P. I., and Geron, C.: Estimates of global terrestrial isoprene emissions using MEGAN (Model of Emissions of Gases and Aerosols from Nature), Atmos. Chem. Phys., 6, 3181–3210, doi:10.5194/acp-6-3181-2006, 2006.

Haeger-Eugensson, M., Moldanova, J., Ferm, M., Jerksjo, M., and Fridell, E.: On the increasing levels of NO_2 in some cities: the role of primary emissions and shipping, Final project report, IVL Report B1886. IVL Swedish Environmental Research Institute Ltd., SE-400 14 Gothenburg, Sweden, 2010.

Jacobson, M. Z.: Air Pollution and Global Warming: History, Science, and Solutions, Cambridge University Press, New York, 2012, 406 pp., 2nd Edn., ISBN 110769115X, 2012.

Johansson, C. and Forsberg, B.: Kvävedioxid och ozon i tätortsluften. Halternas samspel samt konsekvenser för hälsan. Naturvårdsverket, 106 48 Stockholm, rapport 5519. ISBN 91-620-5519-4, 2005.

Karppinen, A., Härkönen, J., Kukkonen, J., Aarnio, P., and Koskentalo, T.: Statistical model for assessing the portion of fine particulate matter transported regionally and long range to urban air, Scand. J. Work Env. Hea., 30, 47–53, 2004.

Karppinen, A., Härkönen, J., Kukkonen, J., Aarnio, P., and Koskentalo, T.: Statistical model for assessing the portion of fine partic-

ulate matter transported regionally and long range to urban air, Scand. J. Work. Env. Hea., 30, 47–53, 2004.

Kauhaniemi, M., Karppinen, A., Härkönen, J., Kousa, A., Koskentalo, T., Aarnio, P., and Kukkonen, J.: Refinement and statistical evaluation of a modelling system for predicting fine particle concentrations in urban areas, in: Proceedings of the 6th International Conference on Urban Air Quality, edited by: Sokhi, R. S. and Neophytou, M., Limassol, Cyprus, 27–29 March 2007, CD-disk: ISBN 978-1-905313-46-4, University of Hertfordshire and University of Cyprus, 68–71, 2007.

Kim, Y., Sartelet K., and Seigneur C.: Comparison of two gas-phase chemical kinetic mechanisms of ozone formation over Europe, J. Atmos. Chem., 62, 89–119, 2009.

Kim, Y., Sartelet, K., and Seigneur, C.: Formation of secondary aerosols over Europe: comparison of two gas-phase chemical mechanisms, Atmos. Chem. Phys., 11, 583–598, doi:10.5194/acp-11-583-2011, 2011.

Liu, X.-H., Zhang, Y., Cheng, S.-H., Xing, J., Zhang, Q., Streets, D. G., Jang, C. J., Wang, W.-X., and Hao, J.-M.: Understanding of Regional Air Pollution over China using CMAQ: – Part 1 Performance Evaluation and Seasonal Variation, Atmos. Environ., 44, 2415–2426, 2010.

MacCarthy, J., Thistlethwaite, G., Salisbury, E., Pang, Y., and Misselbrook, T.: Air Quality Pollutant Inventories for England, Scotland, Wales and Northern Ireland: 1990 – 2010, A report of the National Atmospheric Emissions Inventory, AEA Group, http://uk-air.defra.gov.uk/reports/cat07/1209130947_DA_AQPI_2010_MainBody_v1.pdf, 2012.

Mallet, V. and Sportisse, B.: Uncertainty in a chemistry-transport model due to physical parameterizations and numerical approximations: An ensemble approach applied to ozone modeling, J. Geophys. Res., 111, D01302, doi:10.1029/2005JD006149, 2006.

Mathur, R., Shankar, U., Hanna, A. F., Odman, M. T., McHenry, J. N., Coats Jr., C. J., Alapaty, K., Xiu, A., Arunachalam, S., Olerud Jr., D. T., Byun, D. W., Schere, K. L., Binkowski, F. S., Ching, J. K. S., Dennis, R. L., Pierce, T. E., Pleim, J. E., Roselle, S. J., and Young, J. O.: Multiscale Air Quality Simulation Platform (MAQSIP): Initial applications and performance for tropospheric ozone and particulate matter, J. Geophys. Res., 110, D13308, doi:10.1029/2004JD004918, 2005.

Monks, P. S.: Gas-phase radical chemistry in the troposphere, Chem. Soc. Rev., 34, 376–395, 2005.

Norman, M. and Johansson, C.: Studies of some measures to reduce road dust emissions from paved roads in Scandinavia, Atmos. Environ., 40, 6154–6164, 2006.

Otorepec, P. and Gale, T.: CELJE CITY REPORT, in 2004 ENHIS1 City Reports, European APHEIS project, Institute of Public Health of the Republic of Slovenia, Ljubljana, Slovenia, available at: http://www.apheis.org/ApheisNewCityReports1.PDF/index.html, 2004.

Øystein, H., Sorteberg, A., Schmidbauer, N., Solberg, S., Stordal, F., Simpson, D., Lindskog, A., Areskoug, H., Oyola, P., Lättilä, H., and Heidam, N. Z.: European VOC Emission Estimates Evaluated by Measurements and Model Calculations, J. Atmos. Chem., 28, 173–193, 1997.

Pakkanen, T. A., Loukkola, K., Korhonen, C. H., Aurela, M., Mäkela, T., Hillamo, R. E., Aarnio, P., Koskentalo, T., Kousa, A., and Maenhaut, W.: Sources and chemical composition of atmospheric fine and coarse particles in the Helsinki area, Atmos.

Environ., 35, 5381–5391, 2001b.

Pay, M. T., Jiménez-Guerrero, P., and Baldasano, J. M.: Implementation of resuspension from paved roads for the improvement of CALIOPE air quality system in Spain, Atmos. Environ., 45, 802–807, 2011.

Péré, J. C., Mallet, M., Pont, V., and Bessagnet, B.: Impact of aerosol direct radiative forcing on the radiative budget, surface heat fluxes, and atmospheric dynamics during the heat wave of summer 2003 over western Europe: A modeling study, J. Geophys. Res., 116, D23119, doi:10.1029/2011JD016240, 2011.

Perrino, C. and Putaud, J.-P.: long-term trends in atmospheric pollution in Italy – assessment of the EMEP measurements and modeling work in Europe from 1977 until today, EUR 20979 EN, pp. 19, all also available on the JRC/IES/CCU world wide web site at: http://ccu.ei.jrc.it/ccu/, 2003.

Putaud, J.P., Raes, F., Van Dingenen, R., Bruggemann, E., Facchini, M.C., Decesari, S., Fuzzi, S., Gehrig, R., Huglin, C., Laj, P., Lorbeer, G., Maenhaut, W., Mihalopoulos, N., Mulller, K., Querol, X., Rodriguez, S., Schneider, J., Spindler, G., ten Brink, H., Torseth, K. and Wiedensohler, A.: A European aerosol phenomenology-2: chemical characteristics of particulate matter at kerbside, urban, rural and background sites in Europe, Atmos. Environ., 38, 2579–2595, 2004.

Queen, A. and Zhang, Y.: Examining the sensitivity of MM5-CMAQ predictions to explicit microphysics schemes and horizontal grid resolutions, Part III – The impact of horizontal grid resolution, Atmos. Environ., 42, 3869–3881, 2008.

Real, E. and Sartelet, K.: Modeling of photolysis rates over Europe: impact on chemical gaseous species and aerosols, Atmos. Chem. Phys., 11, 1711–1727, doi:10.5194/acp-11-1711-2011, 2011.

Ribeiro, I., Cascão, P., Monteiro, A., Lopes, M., Tavares, R., Figueira de Sousa, J., Miranda, A.I., and Borrego, C.: The impact of biodiesel on air pollutant emissions: Northern Portugal case study, In the IAIA12 Conference Proceedings' Energy Future The Role of Impact Assessment 32nd Annual Meeting of the International Association for Impact Assessment 27 May–1 June 2012, Centro de Congresso da Alfândega, Porto – Portugal, 2012.

Roustan, Y., Sartelet, K. N., Tombette, M., Debry, É., and Sportisse, B.: Simulation of aerosols and gas-phase species over Europe with the WRF/Polyphemus system. Part II: Model sensitivity analysis for 2001, Atmos. Environ., 44, 4219–4229, 2010.

Sartelet, K., Hayami, H., and Sportisse, B.: MICS-Asia Phase I: Model-to-data comparison for 2001, Atmos. Environ., 41, 6116–6131, doi:10.1016/j.atmosenv.2007.03.005, 2007.

Sartelet, K. N., Couvidat, F., Seigneur, C., and Roustan, Y.: Impact of biogenic emissions on air quality over Europe and North America, Atmos. Environ., 53, 131–141, 2012.

Simpson, D., Winiwarter, W., Brjesson, G., Cinderby, S., Ferreiro, A., Guenther, A., Hewitt, C., Janson, R., Khalil, M., Owen, S., Pierce, T., Puxbaum, H., Shearer, M., Skiba, U., Steinbrecher, R., Tarrason, L., Oquist, M.: Inventorying emissions from nature in Europe, J. Geophys. Res., 104, 8113–8152, 1999.

SLB-analys: The Stockholm Trial, Effects on air quality and health, ISSN 1400-0806, City of Stockholm Environment and Health Administration, Tekniska nämndhuset, Fleminggatan 4. Box 8136 SE-104 20 Stockholm SWEDEN, 2006.

Sogacheva, L., Dal Maso, M., Kerminen, V.-M. and Kulmala, M.: Probability of nucleation events and aerosol particle

concentration in different air mass types arriving at Hyytiälä, southern Finland, based on back trajectories analysis, Boreal Environ. Res., 10, 479–491, 2005.

Tang, L., Chen, D., Karlsson, P.-E., Gu, Y., and Ou, T.: Synoptic circulation and its influence on spring and summer ozone concentrations in southern Sweden, Boreal Env. Res., 14, 889–902, 2009.

Tervahattu, H., Kupiainen, K.J., Räisänen, M., Mäkelä, T., and Hillamo, R.: Generation of urban road dust from anti-skid and asphalt concrete aggregates, J. Hazard. Mater, 132, 39–46, 2006.

Tuccella, P., Curci, G., Visconti, G., Bessagnet, B., Menut, L., and Park, R. J.: Modeling of gas and aerosol with WRF/Chem over Europe: Evaluation and sensitivity study, J. Geophys. Res., 117, D03303, doi:10.1029/2011JD016302, 2012.

Valari, M. and Menut, L.: Does an increase in air quality models' resolution bring surface ozone concentrations closer to reality?, J. Atmos. Oceanic Technol., 25, 1955–1968, 2008.

Vallius, M., Lanki, T., Tiittanen, P., Koistinen, K., Ruuskanen, J. and Pekkanen, J., Source apportionment of urban ambient $PM_{2.5}$ in two successive measurement campaigns in Helsinki, Finland, Atmos. Environ., 37, 615–623, 2003.

van Aardenne, J. A., Dentener, F. J., Olivier, J. G. J., Peters, J. A. H. W. and Ganzeveld, L. N.: The EDGAR 3.2. Fast Track dataset (32FT2000). Documentation and datasets available at: http://www.mnp.nl/edgar/model/v32ft2000edgar/, 2007.

Wolke, R., Schröder, W., Schrödner, R., and Renner, E.: Influence of grid resolution and meteorological forcing on simulated European air quality: A sensitivity study with the modeling system COSMO-MUSCAT, Atmos. Environ., 53, 110–130, 2012.

Zhang, Y., Liu, P., Pun, B., and Seigneur, C.: A Comprehensive Performance Evaluation of MM5-CMAQ for the Summer 1999 Southern Oxidants Study Episode, Part III, Diagnostic and Mechanistic Evaluations, Atmos. Environ., 40, 4856–4873, 2006.

Zhang, Y., Wen, X.-Y., and Jang, C. J.: Simulating Climate-Chemistry-Aerosol-Cloud-Radiation Feedbacks in Continental US using Online-Coupled WRF/Chem, Atmos. Environ., 44, 3568–3582, 2010.

Zhang, Y., Chen, Y.-C., Sarwar, G., and Schere, K.: Impact of Gas-Phase Mechanisms on WRF/Chem Predictions: Mechanism Implementation and Comparative Evaluation, J. Geophys. Res., 117, D1, doi:10.1029/2011JD015775, 2012a.

Zhang, Y., Karamchandani, P., Glotfelty, T., Streets, D. G., Grell, G., Nenes, A., Yu, F.-Q., and Bennartz, R.: Development and Initial Application of the Global-Through-Urban Weather Research and Forecasting Model with Chemistry (GU-WRF/Chem), J. Geophys. Res., 117, D20206, doi:10.1029/2012JD017966, 2012b.

Zhang, Y., Sartelet, K., Wu, S.-Y., and Seigneur, C: Application of WRF/Chem-MADRID and WRF/Polyphemus in Europe – Part 1: Model description, evaluation of meteorological predictions, and aerosol-meteorology interactions, Atmos. Chem. Phys., 13, 6807–6843, doi:10.5194/acp-13-6807-2013, 2013.